INTERNATIONAL MARITIME ORGANIZATION

IMO

E

SUB-COMMITTEE ON STABILITY AND LOAD LINES AND ON FISHING VESSELS SAFETY
51st session
Agenda item 4

SLF 51/INF.3
11 April 2008
ENGLISH ONLY

REVISION OF THE INTACT STABILITY CODE

New generation intact stability criteria

Submitted by Germany

SUMMARY

Executive summary:	Research has been undertaken in matters of cargo loss and damage on container ships due to parametric and synchronous rolling. Included is information on the validation of numerical tools, considerations regarding criteria related to cargo loss and damage, testing of different procedures for design assessment and a methodology for on-board guidance
Strategic direction:	5.2
High-level action:	5.2.1
Planned output:	5.2.1.2
Action to be taken:	Paragraph 9
Related documents:	SLF 50/WP.2 and SLF 50/INF.2

Introduction

1 The Sub-Committee, at its fiftieth session, approved the updated plan of action for matters related to intact stability, proposed by the IS Working Group (SLF 50/WP.2, annex 6).

2 In paragraph 2.4.3 of the aforementioned updated plan of action, the plan aims at the development of procedures for direct assessment (as part or as alternative for published criteria) of stability failures caused by parametric resonance, including consideration of matters related to large accelerations and loads on cargo and stability variation in waves.

3 Furthermore, in paragraph 2.5.1, the plan aims at the development of standard requirements for on-board guidance.

4 The difficult task of developing procedures for direct assessment and standard requirements for on-board guidance for the different types and modes of stability failures requires a co-ordinated effort of all participating delegations, open discussion and exchange of information on the relevant activities in the member countries.

Work on new generation intact stability criteria

5 At SLF 50, Germany submitted a document SLF 50/INF.2, outlining the general approach towards the development of the new generation intact stability criteria, and proposing some ideas for particular problems.

6 The work towards the development of procedures for direct assessment and on-board guidance has been continued after SLF 50, in accordance with the updated plan of action for matters related to intact stability.

7 This research paper deals with the specific problem of cargo loss and damage on container ships due to parametric and synchronous rolling, as set out in the annex, including:

.1 additional validation of numerical tools which can be used in the procedures for direct assessment and for the development of on-board guidance;

.2 considerations regarding criteria related to cargo loss and damage to container ships;

.3 testing of different procedures for design assessment; and

.4 a methodology for the development of on-board guidance.

8 Notwithstanding the fact that the complete development of the procedures for direct assessment and requirements for on-board guidance requires much more time and effort, Germany is of the opinion that the submitted document might be a useful contribution to the activities of the working group towards new generation intact stability criteria, and contains useful information for further discussion in the working group.

Action requested of the Sub-Committee

9 The Sub-Committee is invited to consider the information provided in the above and the annex, and to take action as appropriate.

***

ANNEX

TECHNICAL NOTES ON DESIGN ASSESSMENT PROCEDURE AND OPERATIONAL GUIDANCE FOR AVOIDANCE OF CARGO LOSS AND DAMAGE IN HEAVY WEATHER

1. List of Definitions

General Parameters

Fr	$v/\left(gL_{pp}\right)^{1/2}$	Froude number	
g		acceleration of gravity	m/s^2

Ship Geometry

B	moulded breadth at waterline	m
G	centre of gravity of a vessel	
GM	transverse metacentric height (distance from the centre of gravity to the metacentre), corrected for free surface effects	m
KG	distance from the centre of gravity to the keel	m
KT	distance from the top of container stack to the keel	m
L_{oa}	length overall	m
L_{pp}	length between perpendiculars	m
L_{CG}	horizontal distance from the aft perpendicular to the centre of gravity	m
T	moulded draught of ship hull at midship	m
T_{ap}	draught at aft perpendicular	m
T_{fp}	draught at forward perpendicular	m
V	displacement volume	m^3

Ship Masses

I	I^s+I^h	total moment of inertia (^{s} dry, ^{h} added)	kg·m^2
I_{xx}	$I^s_{xx}+I^h_{xx}$	total roll moment of inertia around the principal axis x	kg·m^2
I_{xz}	$I^s_{xz}+I^h_{xz}$	total mixed moment of inertia in case of non-principal axes	kg·m^2
I_{zz}	$I^s_{zz}+I^h_{zz}$	total yaw moment of inertia	kg·m^2
k_{xx}	$\left(I_{xx}/m\right)^{1/2}$	roll radius of gyration around the principal axis x	m
m		ship mass	kg

Ship Motions

ω_φ	$2\pi/T_\varphi$	circular natural frequency of roll	Hz
T_φ		natural period of roll	s
v		speed of the ship	m/s
ϑ		angle of pitch or trim	rad
φ		angle of roll or heel	rad
ψ		yaw angle	rad

Seaway

h_s		significant wave height	m
h_w		regular wave height	m
λ_w		wave length	m
T_e		wave encounter period	s
T_p		peak wave period	s
T_z		wave period by zero up-crossing	s
T_1		mean seaway period	s
T		regular wave period	s
μ		wave encounter angle	rad
ω_e	$2\pi/T_e$	circular wave encounter frequency	Hz
ω	$2\pi/T$	circular wave frequency	rad/s

Statistics

E_x	expectation, population mean of a random quantity x
F_x	cumulative probability distribution of a random quantity x
f_x	probability density of a random variable x
σ_x	standard deviation of a random quantity x
E_t	expected upcrossing period
τ	sample estimation of the expected upcrossing period

Subscripts

0	initial
ap	aft perpendicular
fp	fore perpendicular
φ	heel, roll
ϑ	trim
z	heave
w	wave

Superscripts

a	amplitude
s	ship
h	hydrodynamic

2. Introduction

Modern container ships are susceptible to cargo losses and damages. This is partly due to the hull form (e.g. large bow flare and overhanging stern, which can lead to parametric rolling), and partly due to the lack of operational guidance supplied to the master. In addition, the tendency of increasing ship sizes and changing main dimensions, as wells as their typical relations for container ships built now and expected to be built in the near future may challenge the established experience of ship designers and operators. All these factors can increase the danger of dynamic stability problems leading to cargo losses and damages. Loss and damage of cargo lead to economic loss as well as pollution and contamination of the environment.

A large share of reported cargo damages and losses is due to heavy weather. The problem is amplified by the lack of operational guidance. Therefore, the aim of these guidelines is to propose

- procedures to assess new designs of container ships with regard to excessive motions and accelerations, and
- methodology for ship-specific operational guidance helping the ship master to avoid excessive motions and accelerations in heavy seas.

Both developments use numerical simulations of ship motions in seaway. Design assessment is based on calculated probabilistic measures of cargo safety for selected critical scenarios, while operational guidance is based on the identification of the combinations of operational parameters leading to excessive motions for seaways and loading conditions expected in the ship's lifetime.

3. Example Ships

The following container ships are used in the study (see Table 1 for general data):

- a 12770 TEU container ship (further referred to as Ship A) for four load cases with GM=2.68, 3.8, 4.57 and 5.88 m
- a 8400 TEU container ship (Ship B) for GM=0.88, 1.26, 1.95, 3.797 and 7.5 m
- a feeder container ship (Ship C) for GM=0.67, 0.82, 1.71 and 2.54 m

Table 1: General data for the load cases used in the study

	ship A				ship B					ship C			
GM, m	2.68	3.8	4.57	5.88	0.88	1.26	1.95	3.797	7.5	0.67	0.82	1.71	2.54
T_φ, s	29.089	25.032	22.52	19.513	40.8	32.057	25.438	18.589	12.442	18.372	16.711	11.701	9.741
v, knots	25.42	25.42	25.42	25.42	23.32	23.32	23.32	23.32	23.32	17.0	17.0	17.0	17.0
L_{oa}, m	382.0	382.0	382.0	382.0	331.9	332.0	331.8	332.0	324.3	117.9	117.9	117.9	117.9
L_{pp}, m	366.2	366.2	366.2	366.2	318.8	317.3	318.8	317.3	318.8	108.0	108.0	108.0	108.0
B, m	54.2	54.2	54.2	54.2	43.2	43.2	43.2	43.2	43.2	17.9	17.9	17.9	17.9
T_{fp}, m	14.32	14.385	12.975	14.695	12.97	14.238	14.09	12.728	9.66	7.11	6.86	7.45	4.39
T_{ap}, m	15.5	15.155	14.025	15.245	14.89	14.647	14.88	12.949	13.06	7.1	7.09	6.76	5.03
KG, m	24.462	23.437	23.3	21.233	19.48	19.499	18.95	16.797	14.02	7.464	7.305	6.376	5.501
L_{CG}, m	168.689	169.705	170.866	169.932	150.35	152.016	156.69	152.608	148.73	54.213	53.957	55.149	54.138
m, t	$2.062\cdot10^5$	$2.032\cdot10^5$	$1.809\cdot10^5$	$2.065\cdot10^5$	$1.348\cdot10^5$	$1.393\cdot10^5$	$1.409\cdot10^5$	$1.208\cdot10^5$	$1.05\cdot10^5$	$9.77\cdot10^3$	$9.553\cdot10^3$	$9.737\cdot10^3$	$5.863\cdot10^3$
I^s_{xx}, t·m^2	$9.418\cdot10^7$	$9.282\cdot10^7$	$8.263\cdot10^7$	$9.429\cdot10^7$	$3.569\cdot10^7$	$3.832\cdot10^7$	$4.087\cdot10^7$	$3.324\cdot10^7$	$2.353\cdot10^7$	$5.009\cdot10^5$	$4.898\cdot10^5$	$5.03\cdot10^5$	$3.006\cdot10^5$
I^s_{yy}, t·m^2	$1.783\cdot10^9$	$1.757\cdot10^9$	$1.564\cdot10^9$	$1.785\cdot10^9$	$8.557\cdot10^8$	$9.111\cdot10^8$	$9.22\cdot10^8$	$7.903\cdot10^8$	$6.049\cdot10^8$	$7.122\cdot10^6$	$6.964\cdot10^6$	$7.229\cdot10^6$	$4.274\cdot10^6$
I^s_{zz}, t·m^2	$1.791\cdot10^9$	$1.765\cdot10^9$	$1.571\cdot10^9$	$1.793\cdot10^9$	$8.563\cdot10^8$	$9.183\cdot10^8$	$8.951\cdot10^8$	$7.965\cdot10^8$	$6.668\cdot10^8$	$7.122\cdot10^6$	$6.964\cdot10^6$	$7.226\cdot10^6$	$4.274\cdot10^6$

4. Overview of Dynamic Stability Problems

4.1. Introduction

The aim of these guidelines is to reduce the danger of parametric resonance (low-cycle and fundamental) and synchronous rolling, which may lead to cargo loss or damage for container ships.

4.2. Synchronous Rolling

Synchronous rolling occurs if a ship is excited close to its natural roll frequency by waves approaching from the directions close to beam seas. Note that natural roll frequency changes both due to waves and due to ship motions, see e.g. Fig. 7. For container ships, synchronous rolling is relevant for load cases with relatively large GM.

4.3. Low-Cycle Parametric Resonance

Parametric resonance is a gradual build-up of rolling when righting levers vary in resonance with natural roll motions. Righting levers oscillate due to change in time of the submerged hull geometry, caused by waves or due to heave and pitch motions. Low-cycle resonance (also called principal resonance) occurs when the wave encounter period is close to half the natural roll period, so that the righting levers attain minimum twice during a roll period.

4.4. Fundamental Parametric Resonance

The fundamental parametric resonance ($T_e \approx T_\varphi$) is also believed to be important. Here, the restoring attains minimum once during each roll period. Therefore a ship rolls more to the leeward side in phase with the wave crest amidships and less back to windward when located in the wave trough.

5. Description of Numerical Tool rolls

5.1. Introduction

The method rolls (roll simulation) was established by *Söding (1982)* and further developed by *Kröger (1987)* and *Petey (1986)*. It was distributed to different universities and companies in the 1990s and has undergone continuous development since then.

The simulations are very fast, so that rolls can be used routinely even for studies involving a large number of seaways and ship operation conditions and long simulation times.

The method was developed to simulate accurately the roll motion whereas other motions are treated primarily to take account of their influence on roll, because methods not including the influence of the other degrees of freedom on the roll motion cannot predict correctly roll motions in steep waves. The degrees of freedom are separated into two groups:

- those for which hydrodynamic effects are small but forces and moments depend strongly nonlinearly on wave and motion amplitudes (roll and surge motions) and
- those for which nonlinear effects are less important (heave, pitch, sway and yaw).

For these different groups of motions, different computational methods are applied. Heave, pitch, sway and yaw motions are computed in the frequency domain using a linear strip method; from the motion transfer functions found in this way, the motion history in an irregular seaway is found superimposing reactions to harmonic waves. For the surge and roll, the relatively small hydrodynamic effects are only roughly approximated, while the nonlinear hydrostatic and Froude-Krylov forces are approximated by more accurate models.

5.2. Roll Motion Equation

The equation of roll motion is

$$\vec{M} = d\vec{H}/dt\,, \tag{1}$$

where $\vec{M}$ is the moment by external forces and $\vec{H}$ is the angular momentum of the ship. Both quantities are described in a coordinate system ξ,η,ζ, the orientation of which is defined with respect to the horizon (ζ points downward, ξ into the average forward direction of the ship), and its origin is fixed in the centre of gravity G of the ship's mass.

Another coordinate system x,y,z is used which is fixed to the ship and participates in its rotations; the axes point forward, to starboard and down, respectively. Its origin is assumed in the midship section and midship plane at the height of the keel.

The coordinates $[\xi,\eta,\zeta]^T$ in the first coordinate system of the vector $\vec{\xi}$ from the origin G to a point, and the column of the coordinates $[x,y,z]^T$ expressed in the second coordinate system of the vector $\vec{x}$ from the origin K of the second system to the same point are related by the equation

$$[\xi,\eta,\zeta]^T = \mathbf{T}\cdot[x,y,z]^T + [\xi_K,\eta_K,\zeta_K]^T\,, \tag{2}$$

where **T** is a 3×3 matrix, which depends on the heel angle φ, trim angle θ and yaw angle ψ. Consistently with other approximations, **T** is linearised with respect to θ and ψ but not φ:

$$\mathbf{T} = \begin{bmatrix} 1 & \theta\sin\varphi - \psi\cos\varphi & \theta\cos\varphi + \psi\sin\varphi \\ \psi & \cos\varphi & -\sin\varphi \\ -\theta & \sin\varphi & \cos\varphi \end{bmatrix}. \tag{3}$$

The angular momentum is defined as

$$\vec{H} = \int_{\text{all masses}} \vec{\xi} \times \frac{\mathrm{d}\vec{\xi}}{\mathrm{d}t}\,\mathrm{d}m\,. \tag{4}$$

Combining (1) to (4) gives, after linearisation with respect to θ and ψ, for a symmetric mass distribution, the following heel moment in the system ξ,η,ζ:

$$\begin{aligned} M_\xi = {} & \left[I_{Gx} - I_{Gxz}\left(\psi\sin\varphi + \theta\cos\varphi\right)\right]\ddot{\varphi} \\ & + I_{Gxz}\left[\sin\varphi\left(\ddot{\theta} + \theta\dot{\varphi}^2\right) - \cos\varphi\left(\ddot{\psi} + \psi\dot{\varphi}^2\right)\right], \end{aligned} \tag{5}$$

where $I_{G\ldots}$ are the mass moments of inertia referred to the centre of gravity G:

$$\begin{aligned} I_{Gx} &= \int\left[\left(y - y_G\right)^2 + \left(z - z_G\right)^2\right]\mathrm{d}m\,, \\ I_{Gxz} &= \int\left(x - x_G\right)\left(z - z_G\right)\mathrm{d}m. \end{aligned} \tag{6}$$

The heeling moment M_ξ is calculated as a sum of the following contributions:

Moment due to Roll Acceleration: the added moment of inertia I_{xx}^h due to the acceleration of the surrounding fluid gives a contribution

$$M_I = -I_{xx}^h\ddot{\varphi}\,, \tag{7}$$

where, I_{xx}^h (with respect to the central longitudinal axis) is determined by potential flow calculations.

Damping Moment: this is assumed to consist of a linear and a quadratic term:

$$M_D = -b_L\dot{\varphi} - b_Q\dot{\varphi}\left|\dot{\varphi}\right|. \tag{8}$$

The coefficients can be found either from model data (see e.g. *Blume (1979)*) or empirical approximations.

Weight: because the moment reference point is *G*, the weight does not contribute to M_ξ.

Froude-Krylov Moment: due to the pressure in still water or in a wave, not modified by the ship. This contribution is related to the righting-arm curve, including its changes in waves. The program uses stored tables of righting arms calculated hydrostatically in a wave-shaped water surface. This procedure uses the concept of Grim's equivalent wave (see *Grim (1961)*): in a natural seaway, the irregular water surface which would occur along the midship plane if the ship were not present is approximated within the length range of the ship by a suitable standard shape, which produces approximately the same righting moment curve over heel as the real irregular water surface. As such a standard shape, the following expression for ζ is used (this expression was generalised by *Söding* compared to *Grim*'s approach):

$$\zeta\left(x,t\right) = a\left(t\right) + b\left(t\right)x + c\left(t\right)\cos\left(2\pi x/\lambda\right). \tag{9}$$

The formula contains a length-averaged increase or decrease $a(t)$ of the free surface height with respect to the average water level, a length-averaged lengthwise slope of the water surface $b(t)$ and a wavy shape with amplitude $c(t)$. The wave crest or trough is assumed at the mid-ship section, and the wavelength λ is selected constant for a given ship, in most cases equal to the ship length or slightly larger, because waves of such a length have the most significant influence on the righting levers.

The time functions $a(t)$, $b(t)$ and $c(t)$ are computed from the transfer functions between these quantities and the regular waves constituting the seaway. Before starting the simulation, these transfer functions are determined using the least-square method (see *Kröger (1987)*). A reduction factor e^{-kz} may be applied to account for the smaller pressure variations along the ship's bottom than at the water surface (Smith effect).

Before starting the simulations, righting arms are determined depending on draft d, trim angle θ, heel φ and wave amplitude c. For each time instant within the simulation, the heave motion ζ_K and the pitch motion θ are determined, using transfer functions computed by a strip method. For interpolating the righting arm h from the table, actual values of draft and trim are determined as

$$d = \text{average ship draft} - a + \zeta_K\,, \tag{10}$$

$$\tau = \text{average trim} - b + \theta\,. \tag{11}$$

These give the following moment due to heel in wave:

$$M_A = -\rho g V h\,, \tag{12}$$

where V is the actual displacement corresponding to the instantaneous draft and trim of the ship.

Denoting by m_{zz}^h the added mass for heave motion, we have approximately (neglecting coupling with the other motions)

$$\left(m + m_{zz}^h\right)\ddot{\zeta}_K = -\rho g V + mg\,, \tag{13}$$

where m is the ship's mass. The value V following from this equation is inserted into (12) giving

$$M_A = -m\left(g - \ddot{\zeta}_K\right)h + m_{zz}^h \ddot{\zeta}_K h\,. \tag{14}$$

Vertical Ship Acceleration: the vertical acceleration of the ship changes the water pressure. The moment caused by this effect depends on the "centre of gravity of the added mass" m_{zz}^h. As an approximation, the centre of gravity B of the displacement volume is used, which gives a moment

$$M_V = -m_{zz}^h \ddot{\zeta}_K h\,, \tag{15}$$

which cancels with the second term in (14), giving

$$M_A + M_V = -m\left(g - \ddot{\zeta}_K\right)h\,. \tag{16}$$

Together with the dependence of h on the wave height c the term $m\ddot{\zeta}_K h$ may contribute to the parametric excitation of roll motions.

Moment M_{SY} due to sway and yaw motions: this contribution is determined by a linear strip method. Before starting a simulation, the transfer function between this moment and the waves is determined.

Moment M_E due to the wave excitation: in computing the moment M_A+M_V, a horizontal water surface is assumed in the transverse direction of the ship. The transverse inclination of the wavy water surface generates then another contribution to the external moment. This moment is also accounted for by a transfer function, computed by the strip theory.

Adding the listed contributions to the external moment gives together with (5) the following ordinary differential equation for the roll angle φ:

$$\begin{aligned}&\left[I_{Gx} + I_x{}'' - I_{Gxz}\left(\psi\sin\varphi + \theta\cos\varphi\right)\right]\ddot{\varphi}\\ &= I_{Gxz}\left[\left(\ddot{\psi} + \psi\dot{\varphi}^2\right)\cos\varphi - \left(\ddot{\theta} + \theta\dot{\varphi}^2\right)\sin\varphi\right]\\ &-\left(d_L + d_Q\left|\dot{\varphi}\right|\right)\dot{\varphi} - m\left(g - \ddot{\zeta}\right)h\left(d,\tau,\varphi,c\right)\\ &+ M_{SY} + M_E + M_W\,.\end{aligned} \tag{17}$$

5.2.1. Surge Motion

The surge motion is simulated using the following motion equation:

$$\ddot{\xi}_G = \frac{T\left(1-t\right) - R + X}{m + m_{xx}^h}\,. \tag{18}$$

Here, $T(1-t)$ is the propeller thrust less thrust deduction, calculated depending on the instantaneous speed and the propeller rate of evolution, R is the ship resistance, which is taken from model tests or assumed proportional to the instantaneous ship speed squared, X is the longitudinal force due to waves, and m_{xx}^h is the added mass for the longitudinal motion.

Blume (1976) showed that the Froude-Krylov force, i.e. the force due to the wave pressure undisturbed by the ship, is nearly exclusively responsible for the surge motion; the longitudinal diffraction forces are negligible for such slender bodies as ships. The Froude-Krylov force can be determined using a simple assumption that, for a given ship section, the buoyancy force is directed normal to the wave contour (with a reduction factor e^{-kz}) and thus contains a longitudinal component.

5.2.2. Integration of Motion Equations

The four ordinary first-order differential equations

$$d\dot{\xi}_G / dt = \text{ r.h.s. of (18)}, \tag{19}$$

$$d\xi_G / dt = \dot{\xi}_G\,, \tag{20}$$

$$d\dot{\varphi} / dt = \text{ r.h.s. according to (17)}, \tag{21}$$

$$d\varphi / dt = \dot{\varphi} \tag{22}$$

are integrated numerically using a fourth-order Runge-Kutta method with a fixed time step size.

5.2.3. Determination of the Linear Wave Responses and Seaway Modelling

The time dependencies of draft d, trim θ, wave height c and the ship motions sway, heave, pitch and yaw are assumed to depend linearly on wave amplitudes and are computed using complex transfer functions $\hat{Y}\left(\omega,\mu\right)$, where ω is the circular wave frequency and μ is the wave direction. The complex transfer functions are computed with the software GL STRIP.

The natural seaway is modelled as a linear superposition of regular harmonic waves; nonlinear effects such as sharper wave crests than wave troughs are neglected. The linear responses $r(t)$ are added from the contributions corresponding to the regular waves making up the seaway as

$$r\left(t\right) = \sum_{n=1}^{N_w} \mathrm{Re}\left[\hat{\zeta}_n \hat{Y}\left(\omega_n,\mu_n\right) e^{i\left(\omega_n t - k_n \xi_G \cos\mu_n\right)}\right]. \tag{23}$$

Here, n is the index of a regular wave characterised by ω_n and μ_n, k_n is the wave number, and $\hat{\zeta}_n$ is the complex amplitude of wave n, determined from the wave spectrum $S_{\zeta\zeta}\left(\omega,\mu\right)$ as

$$\hat{\zeta}_n = e^{i\varepsilon_n}\sqrt{2S_{\zeta\zeta}\left(\omega_n,\mu_n\right)\Delta\omega_n\Delta\mu_n}\,, \tag{24}$$

where ε_n is a random phase angle distributed uniformly between 0 and 2π.

To avoid self-repetition of the generated seaway, the range of frequencies and wave encounter angles is subdivided into a sufficient number of wave components (typically 50 to 100 wave frequencies per wave angle and 7 to 15 wave angles), constituting a non-uniform Cartesian grid. In each cell of this grid, a certain combination of frequency and angle is selected, independent from the other cells, by a random procedure using a constant probability density. The amplitude of the wave is calculated as square root of the integral of the seaway spectrum over the cell. The integrals are calculated to a prescribed high accuracy using adaptive refinement. Usually, the energy spectrum is discretised into components of equal energy. Each simulation is repeated for randomly varying phases, frequencies and wave headings. In all these runs, different wave tracks result, thus sufficient confidence can be expected in a statistical sense, for example with respect to the average exceedance rate of a certain roll angle.

This procedure neglects the nonlinearity of the seaway, namely that wave crests are, on average, sharper and higher than wave troughs. As experience shows, this is tolerable for the applications considered because the wave nonlinearities are far less important than the nonlinearities of the ship responses.

6. Summary of Validation Work

6.1. Introduction

Systematic model tests were undertaken to study

- parametric roll in regular head and stern waves (HSVA, 2006 – see *Brunswig et al. (2006)* for details)
- parametric and synchronous roll in regular waves from all directions (MARIN, 2007)
- parametric rolling in regular head waves (HSVA, 2007)

6.2. Tests in HSVA, 2006

Brunswig et al. (2006) compared roll motions measured in model experiments with simulations by rolls and GL SIMBEL for ship B. Regular head and stern waves were used deviating by 2 to 5 degrees from exactly longitudinal to initiate roll.

The ratio between wave encounter frequency and roll natural frequency was selected near 2 and 1, i.e. where parametric roll may occur. For the frequency ratio 2, parametrically excited roll motions occur already in waves of 2 m height, whereas for the frequency ratio 1 up to wave heights of 8 m no parametric roll motions could be found. For 10 m wave height, rolls showed moderate parametric rolling, whereas GL SIMBEL did not, and the model experiments showed parametric rolling in one of four cases. Thus, 10 m appears to be the limiting wave height above which ship motions without substantial roll become unstable. Fig. 1 shows maximum roll angles from the tests and simulations for 10 m wave height near the frequency ratio 2. Both tools predict well occurrence of parametric roll and roll amplitudes for parametric resonance. There is only one case where rolls showed parametric rolling whereas the experiment and GL SIMBEL did not. Indeed the limits of stability of the non-rolling condition can only be predicted with some accuracy, thus a few cases must be expected where the simulation shows parametric roll whereas the experiment does not and vice versa. Further, near the limit of parametric roll there are conditions in which both a non-rolling and a parametrically excited roll motion are possible, depending on the initial conditions. The reason is the dependence of the natural roll frequency on the roll amplitude: if the ship has already a substantial roll amplitude, the frequency of encounter may match the resonance close enough to increase the rolling further, whereas a ship having a smaller initial roll motion may miss the resonance condition. This sensitivity to initial conditions is only relevant for regular waves, and not if one is interested in average (over large number of simulations) characteristics of ship motions in natural seaway.

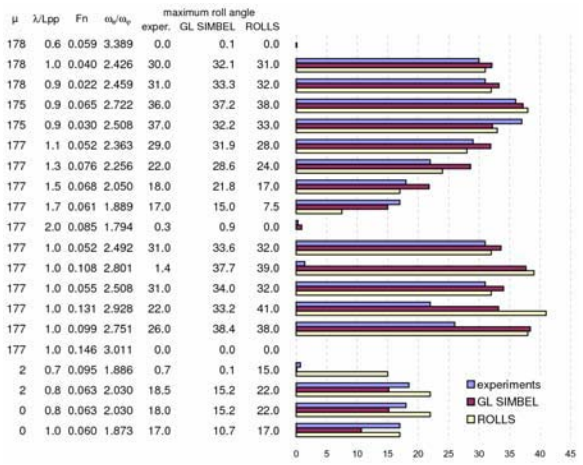

Fig. 1. Comparison of roll amplitudes calculated with rolls and GL SIMBEL with model tests

6.3. Tests in MARIN, 2007

Examples of validation results are shown in Fig. 2 to Fig. 4, indicating the following roll amplitudes:

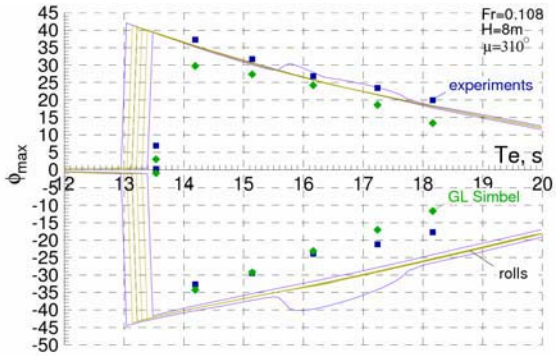

Fig. 2. Low-cycle resonance in stern-quartering waves for ship B with GM=0.88 m, μ=310°, h_w=8.0 m, Fr=0.108

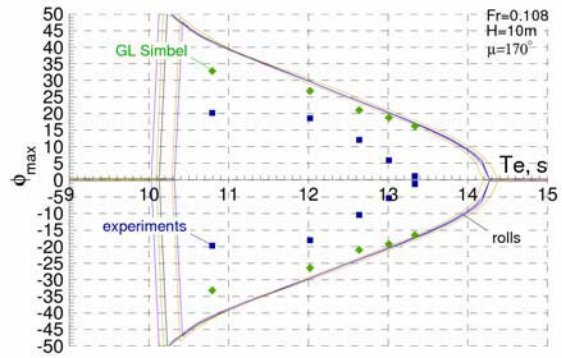

Fig. 3. Low-cycle resonance in bow waves for ship B with GM=1.95 m, μ=170°, h_w=10.0 m, Fr=0.108

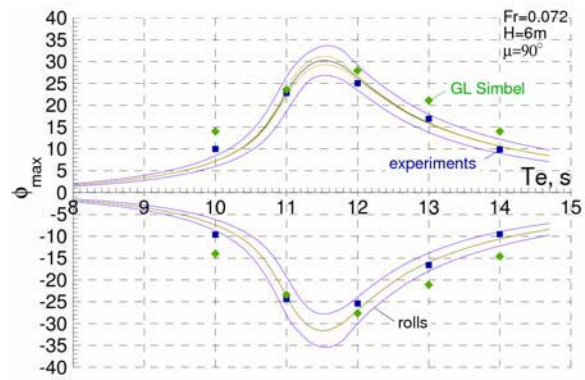

Fig. 4. Synchronous rolling in beam waves for ship B with GM=7.5 m, μ=90°, h_w=6.0 m, Fr=0.072

measurements (blue squares), *calculations with rolls* (lines): an envelope corresponding to calculations with different wave heights and model speeds, within the uncertainty of the experiments, and *calculations with GL SIMBEL* (green diamonds), vs. encounter wave period. Positive values indicate rolling to starboard, negative to port. The corresponding polar plots in axes wave direction-wave period are shown in Fig. 15, Fig. 16 and Fig. 18.

6.4. Tests in HSVA, 2007

23 tests were carried out for ship B with GM=1.26 m in three regular head wave trains with different periods and heights. For each wave train, several runs were done for several model speeds in the range 3 to 15 knots (full scale).

Near the limit of parametric rolling, the roll amplitude is sensitive to small changes in wave heading, wave height, model speed and initial conditions. In some test runs near the limit of parametric roll the length of the basin was not sufficient to reach stationary rolling. Therefore, the model was excited to roll manually with a small disturbance just before entering the wave train. Fig. 5 shows comparison of the measured roll amplitudes (filled symbols) with the results of two types of simulations: one with a long enough simulation time and a large (6°) initial roll angle (lines), and another with the simulation time and the initial disturbance adjusted to the test conditions (empty symbols). Table 2 shows a comparison of the latter type simulation results with measurements.

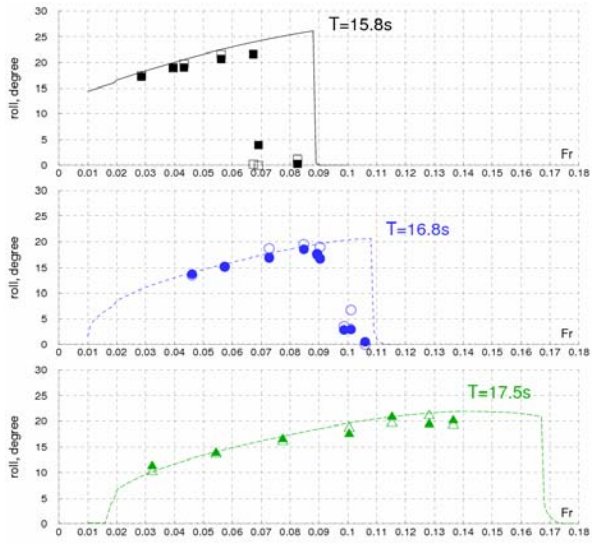

Fig. 5. Calculated and measured roll amplitudes

Table 2. Comparison of calculations with tests

nr.	T, s	T_e, s	h_w, m	v, kts	Fr	roll, degree	
						exp.	calc.
1	16.8	15.300	4.00	5.00	0.0461	13.7	13.5
2	16.8	14.971	3.80	6.23	0.0574	15.2	15.2
3	16.8	14.546	4.00	7.90	0.0728	16.9	18.7
4	16.8	14.232	4.00	9.20	0.0848	18.5	19.5
5	16.8	14.115	3.40	9.70	0.0894	17.6	17.6
6	16.8	14.092	4.00	9.80	0.0904	16.7	19.0
7	16.8	13.886	3.80	10.70	0.0987	2.9	3.5
8	16.8	13.828	4.00	10.96	0.1011	3.0	6.7
9	16.8	13.708	2.60	11.50	0.1060	0.5	0.0
10	15.8	14.841	4.20	3.10	0.0286	17.2	17.5
11	15.8	14.500	3.90	4.30	0.0396	19.0	18.9
12	15.8	14.390	4.06	4.70	0.0433	19.0	19.7
13	15.8	14.017	3.95	6.10	0.0562	20.7	21.5
14	15.8	13.712	3.24	7.30	0.0673	21.6	0.3
15	15.8	13.665	4.00	7.49	0.0691	3.9	0.0
16	15.8	13.313	4.65	8.96	0.0826	0.3	1.2
17	17.5	16.418	7.05	3.50	0.0323	11.3	10.1
18	17.5	15.750	6.54	5.90	0.0544	13.8	13.5
19	17.5	15.110	6.00	8.40	0.0775	16.5	16.0
20	17.5	14.520	6.07	10.90	0.1005	17.5	18.6
21	17.5	14.166	4.60	12.50	0.1153	20.8	19.6
22	17.5	13.870	6.28	13.90	0.1282	19.4	21.0
23	17.5	13.686	5.60	14.80	0.1365	20.1	19.2

7. Factors

7.1. Cargo Loss and Damage

The number of containers lost or damaged per ship per time (e.g. year), i.e. the average rate of container losses per ship, is a suitable measure to characterise cargo safety provided by the ship. On the one hand, it does not depend directly on the duration of the operational life of a ship (this duration is variable and, besides, is not directly related to the average economic consequences of cargo losses). On the other hand, multiplying the average rate of container losses per ship with the number of ships in operation gives the average total number of lost or damaged containers per time, which is an economically sound and convenient measure. Finally, this figure can be easily estimated from the statistics dividing the total number of containers lost or damaged per some time interval by the average number of container ships operating during this time interval.

The average rate of container losses or damages per ship is a product of the rate of container loss or damage events and the average number of containers lost per such event. The last factor depends on the ship size, container allocation, and severity of cargo loss events. To simplify the problem, this factor is not taken into account, i.e. cargo safety is described only by the rate of container loss (or damage) events per ship. This figure can also be derived directly from statistical data. However, using the rate of cargo loss events as the basis for criteria requires caution: for example, the consequences per cargo loss event may increase in the future due to the increasing size of newly built container ships.

For the practical application of seakeeping analysis tools, the event of cargo loss or damage needs to be related to a set of operational factors that can be easily defined from standard seakeeping calculations. The rate of cargo loss or damage events is substituted in the analysis with the rate of exceedance of the corresponding operational standards.

From experience, cargo loss or damage events occur due to large vertical or lateral accelerations or their combination, thus it seems appropriate to use the rate of exceedance of certain levels of vertical and lateral accelerations as the measure of cargo safety, when numerical seakeeping tools are employed.

7.2. Vertical Accelerations

Vertical accelerations are caused mainly by heave and pitch motions of a ship. Because these motions can be assumed as linear with sufficient accuracy, and also Gaussian-distributed in a natural seaway, short-term statistics of vertical accelerations can be derived from linear (panel methods or strip theories) calculations in the frequency domain, applying then e.g. the Rice formula to calculate the exceedance rate of the prescribed acceleration level.

Another important cause of large vertical accelerations is the whipping response of a ship to slamming impacts. Here, both hydrodynamics and statistics are nonlinear and are out of scope of these guidelines. Only lateral accelerations are considered in detail.

7.3. Lateral Accelerations

The maximum level for the lateral accelerations is taken from the *GL's Rules for Classification and Construction* as $0.5g$, which corresponds to a static heel of 30°. Dynamic roll amplitudes corresponding to this lateral acceleration for a rolling ship will be smaller due to the contribution of inertia to the lateral accelerations. Namely, for a rolling ship, lateral acceleration consists of two contributions (see Fig. 6): due to the gravity acceleration $a_y^{(1)} = -g\sin\varphi$, and due to rotational acceleration $a_y^{(2)} = \ddot{\varphi}h$. Here, h is the height of the top container from the roll axis (positive if the top container is above the roll axis). In Fig. 6, R is the trace of the roll axis.

The total lateral acceleration is therefore

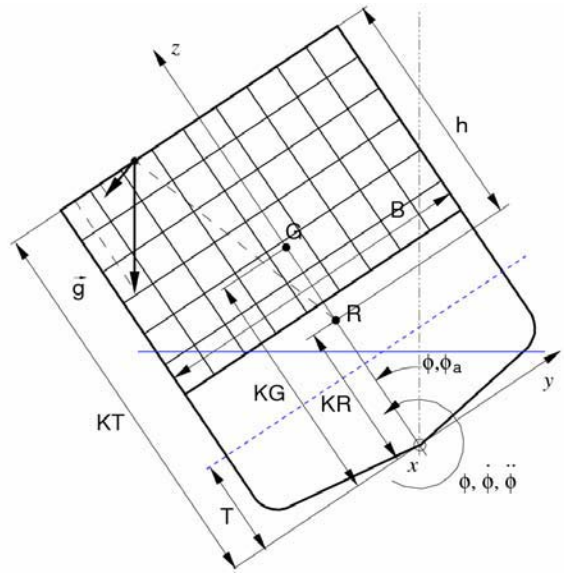

Fig. 6. Acceleration components

$$a_y = a_y^{(1)} + a_y^{(2)} = -g\sin\varphi + \ddot{\varphi}h\,.$$

Assuming harmonic rolling with an amplitude φ_a and circular frequency ω_φ, i.e. roll angle satisfying the dependency $\varphi(t) = \varphi_a \sin\omega_\varphi t$, the instantaneous lateral acceleration becomes

$$a_y = -g\sin\varphi - \varphi_a\omega_\varphi^2 h\sin\omega_\varphi t\,.$$

From the condition that the maximum lateral acceleration $a_y^{\max} = g\sin\varphi_a + \varphi_a\omega_\varphi^2 h$ is less than $g/2$, the equation for the maximum roll amplitude is

$$\sin\varphi_{\max} + \varphi_{\max} h\omega_\varphi^2 / g = 1/2\,. \tag{25}$$

Denote the vertical distance from the top container to keel as KT and the height of the roll axis above the keel as KR. Then $h = KT - KR$, and the equation for the maximum roll angle (25) becomes

$$\sin\varphi_{\max} + \varphi_{\max}\left(KT - KR\right)\omega_\varphi^2 / g = 1/2\,. \tag{26}$$

To find the location of the roll axis, the following empirical formula from *Balcer (2004)* was used:

$$KR = KG - 0.57\left(KG - T\right) - 0.1B\,. \tag{27}$$

Eq. (26) is difficult to use because the natural roll frequency ω_φ depends on the roll amplitude φ_a. To take this factor into account, the dependency $\omega_\varphi(\varphi_a)$ was found from numerical simulations and approximated as a second-order polynomial

$$\omega_\varphi = \omega_{\varphi 0} + A\varphi_a^2\,. \tag{28}$$

The natural frequency of small oscillations $\omega_{\varphi 0}$ and the coefficient A can be defined from dependencies such as shown in Fig. 7 for Ship B. These dependencies are derived from the results of simulations in regular beam waves for a series of wave periods, as plots of the roll amplitude vs. the wave frequency corresponding to the peak response.

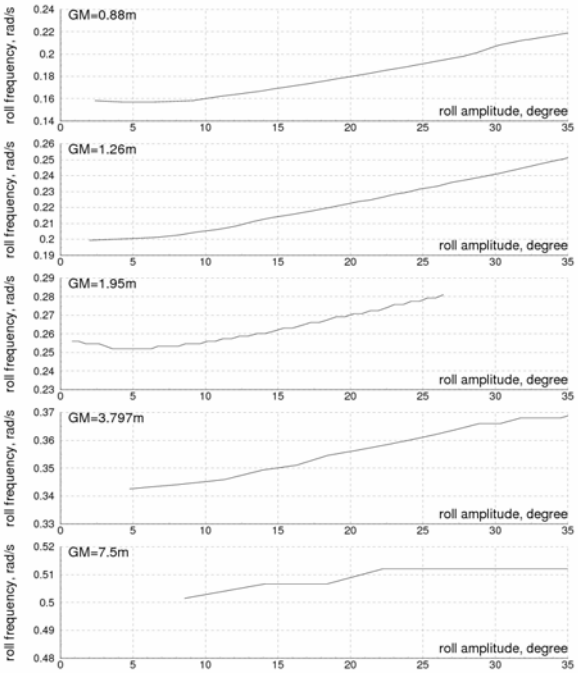

Fig. 7. Natural roll frequency vs. roll amplitude defined from numerical simulations of rolling in regular beam waves

In addition to the 'exact' solution for $\varphi_{\max}$, several simplifications and their combinations were tested:

- ω_φ is taken equal to $\omega_{\varphi 0}$, the natural frequency of small roll oscillations, for all roll amplitudes,
- with a constant $\omega_\varphi = \hat{\omega}_{\varphi 0}$, estimated as

$$\hat{\omega}_{\varphi 0} = \sqrt{(mg \cdot GM)/(1.1 \cdot I^s_{xx})}\,, \tag{29}$$

- linearising $\sin\varphi_{\max}$ as $\varphi_{\max}$, resulting in

$$\varphi_{\max} = 0.5g/\left[g + (KT - KR)\omega_\varphi^2\right]. \tag{30}$$

The discrepancies between the different estimations of the maximum roll amplitude $\varphi_{\max}$ are small. The simplest estimation, based on the linearisation (30) and constant $\omega_\varphi = \hat{\omega}_{\varphi 0}$ according to (29) for all roll amplitudes is close to the 'exact' solution and is also conservative for all of the considered load cases; it is therefore used here. Substituting (29) into (30) gives

$$\varphi_{\max} = \left[2 + 1.8(KT - KR)GM/k^2_{xx}\right]^{-1}. \tag{31}$$

Table 3 shows the results of calculations of $\varphi_{\max}$, including 'exact' and simplified according to (31).

Table 3: Maximum admissible roll amplitude estimated with different methods

	ship A				ship B					ship C			
GM, m	2.68	3.8	4.57	5.88	0.88	1.26	1.95	3.797	7.5	0.67	0.82	1.71	2.54
KT, m	53.4	53.4	53.4	53.4	53.55	53.55	53.55	53.55	53.55	17.2	17.2	17.2	17.2
KR, m	19.017	18.497	17.691	17.663	16.315	16.467	16.164	14.541	12.505	7.257	7.114	6.791	5.050
A	0.0379	0.0363	0.0291	0.0184	0.0943	0.0850	0.0743	0.0542	0.0000	0.1210	0.1406	0.1046	0.0964
$\omega_{\varphi 0}$, rad/s	0.216	0.251	0.279	0.322	0.154	0.196	0.247	0.338	0.505	0.342	0.376	0.537	0.645
$\hat{\omega}_{\varphi 0}$, rad/s	0.229	0.272	0.299	0.339	0.168	0.202	0.251	0.351	0.546	0.341	0.378	0.543	0.665
'exact' $\varphi_{\max}$, deg	25.1	23.7	22.6	21.1	26.5	25.1	23.3	19.7	13.9	26.0	25.2	22.0	18.9
$\varphi_{\max}$ from (31), deg	24.2	22.7	21.5	20.2	25.9	24.8	23.0	19.2	13.3	25.6	25.0	21.8	18.5

8. Criteria and Standards

The exceedance rate r of the prescribed roll angle $\varphi_{\max}$ (the number of exceedance events per time) depends on the seaway conditions $\mathbf{S} = [h_s, T_1]^T$, operational parameters $\mathbf{R} = [v, \mu]^T$ and loading state $\mathbf{L} = [T, \vartheta_s, KG, k_{xx}]^T$. These variables change in time, therefore the expected exceedance rate also changes. Subdivide the continuum of seaway conditions, operational parameters and loading states into a finite number of the ranges of seaway conditions $\mathbf{S}_i$, operational parameters $\mathbf{R}_l$ and loading states $\mathbf{L}_j$. Within each of these ranges the components of $\mathbf{S}$, $\mathbf{R}$ and $\mathbf{L}$ are considered constant, therefore, the expected exceedance rate is also constant.

The probability of an exceedance event occurring during an infinitely small time interval Δt near a randomly selected time instant t is a composite probability, calculated as

$$\Delta p = \sum_i \sum_l \sum_j p(\mathbf{L}_j)\, p(\mathbf{S}_i \mid \mathbf{L}_j) \cdot p(\mathbf{R}_l \mid \mathbf{S}_i, \mathbf{L}_j)\, r(\mathbf{S}_i, \mathbf{R}_l, \mathbf{L}_j)\, \Delta t,$$

then the long-term exceedance rate $r_L = \Delta p / \Delta t$ is

$$r_L = \sum_j p(\mathbf{L}_j) \sum_i p(\mathbf{S}_i \mid \mathbf{L}_j) \cdot \sum_l p(\mathbf{R}_l \mid \mathbf{S}_i, \mathbf{L}_j)\, r(\mathbf{S}_i, \mathbf{R}_l, \mathbf{L}_j).$$

The long-term probabilities of encountering certain discrete situations can be calculated as, e.g. for seaways $p(\mathbf{S}_i) = T_i / T$, where T_i is the total duration of the seaway condition in the range $\mathbf{S}_i$ during a reference time T.

Note that in this summation, only those load cases should be considered that can lead to cargo loss or damage. The probability of certain load cases may vary significantly between different ships or even for the same ship if the route changes. Therefore, the design assessment procedure should be applied to each relevant load case separately.

The probability $p(\mathbf{S}_i)$ of encountering a seaway in the range $\mathbf{S}_i$ with sizes Δh_s and ΔT_1 is equal to $f_{h_s,T_1}\Delta h_s \Delta T_1$, where f_{h_s,T_1} is the probability density function of long-term distribution of significant wave height and mean wave period. This probability density function is calculated here from the annual average probabilities for the North Atlantic from *Söding (2001)* or winter-average probabilities for the same area according to diagram Nr. 19 from *IACS Rec. No.34 (2001)*, by dividing the entries (probabilities) with the size of the cells Δh_s, ΔT_1.

Parametric and synchronous rolling are usually stronger for low speeds and decrease with increasing forward speed. It is possible that a designer chooses to reduce the danger of excessive roll motions by designing a hull form which allows large forward speed to be achieved even in a heavy seaway. Therefore, it seems appropriate to assess designs for the maximum speed possible for given seaway and load case, $v_{\max} = v_{\max}(h_s, T_1, \mu)$. This speed should be defined taking account of the increased resistance in waves, as well as voluntary speed reduction undertaken to avoid, for example, large vertical accelerations, slamming and propeller racing.

Define $r_f(h_s, T_1, \mu, v_{\max}) = f_{h_s,T_1} r(h_s, T_1, \mu, v_{\max})$. Design assessment reduces then to the calculation of the sum $\sum_{h_s,T_1,\mu} r_f(h_s, T_1, \mu, v_{\max})\Delta h_s \Delta T_1 \Delta\mu$ and comparison of the result with a prescribed standard. Instead of this, a quicker procedure is proposed: to find critical conditions, i.e. a combination of h_s, T_1 and μ which maximises r_f:

$$r_f^{\max} = \max_{h_s,T_1,\mu} r_f(h_s, T_1, \mu, v_{\max}) = r_f\left(h_s^*, T_1^*, \mu^*, v_{\max}(h_s^*, T_1^*, \mu^*)\right),$$

and require that for each considered load case, the criterion $r_f^{\max}$ does not exceed a certain standard R_1:

$$r_f^{\max} < R_1. \qquad (32)$$

Load cases not satisfying this condition require operational guidance. For operational guidance, the principle is to avoid combinations of operational parameters for which

$$r_f = f_{h_s,T_1} r(h_s, T_1, \mu, v) > R_2. \qquad (33)$$

In principle, the standards on the r.h.s. of design assessment (32) and operational guidance (33) rules may differ. The following simple way can be used: to select certain load cases for several container ships, which are (e.g. according to experience) sufficiently safe for cargo and calculate $r_f^{\max}$ from numerical simulations for each of these load cases. The load case with the maximum value of $r_f^{\max}$ is selected as the *standard load case*, and $r_f^{\max}$ for this standard load case is set as the standard R_1 for the right-hand side of rule (32). R_2 was set to $10^{-2} R_1$.

A better way to select the standards is to use cost-benefit analysis: R_1 should maximise the difference between average earnings and average cost of lost and damaged containers per time.

9. Physical Aspects of Parametric and Synchronous Rolling

9.1. Critical Areas of Operational Parameters and Seaway Conditions

It is usually assumed that the most critical conditions for parametric rolling occur in waves propagating along the ship, i.e. head and stern waves. Reconsidering these conditions, it seems that oblique wave conditions may be more dangerous for parametric resonance for certain load conditions and forward speeds. The following conditions are proposed for parametric resonance:

- *resonance condition:* encounter wave period T_e should be close to the half of the natural roll period T_φ (for low-cycle resonance) or to the natural roll period (for fundamental parametric resonance)
- *wave length condition:* to produce sufficiently large oscillations of righting levers, ship bow and stern should lie in wave troughs when mid-ship section is on a wave crest and vice versa.

The conditions for synchronous rolling are:

- *resonance condition:* encounter wave period T_e close to the natural roll period T_φ
- *wave direction:* waves should be sufficiently close to beam direction – how close, depends on the wave steepness and the ship's susceptibility to synchronous rolling.

Now find the combinations of wave frequency ω and wave direction μ leading to a given encounter frequency ω_e ($\omega_e = \omega_\varphi$ for synchronous rolling and fundamental parametric resonance or $2\omega_\varphi$ for low-cycle parametric resonance):

1. ship in head waves, or in long following waves overtaking the ship:
   $$\omega = \left(g - \sqrt{g^2 - 4gv\omega_e \cos\mu}\right) \Big/ (2v\cos\mu),$$
   with the limit $\omega \to \omega_e$ for $\mu \to \pm\pi/2$
2. the ship is overtaken by shorter following waves:
   $$\omega = \left(g + \sqrt{g^2 - 4gv\omega_e \cos\mu}\right) \Big/ (2v\cos\mu).$$

For following waves in cases 1 and 2, the limitation applies $\omega_e < g/(4v\cos\mu)$, leading to the following condition for the wave encounter angle:

$\cos^{-1}\left[g/(4v\omega_e)\right] < \mu < \pi/2$ for $v > g/(4\omega_e)$ or $\mu < \pi/2$ otherwise.

3. the ship overtakes short following waves, $\omega = \left(g + \sqrt{g^2 + 4gv\omega_e \cos\mu}\right)/(2v\cos\mu)$, for $-\pi/2 < \mu < \pi/2$.

The lines for which these conditions are satisfied (resonance lines) are shown in axes T (radial coordinate) – μ (circumferential) in Fig. 8 and Fig. 9 for $\omega_e = 2\omega_\varphi$ and ω_φ, respectively, for Ship B with *GM*=3.797 m, for seven uniformly distributed speeds from 0 to 23.3 knots. Two lines are shown for each speed: solid line corresponding to bow waves and overtaking stern waves (conditions 1 and 2) and dashed one corresponding to stern waves overtaken by the ship (condition 3). The latter condition leads to very short waves, which do not represent a danger in a real seaway.

For conditions 1 and 2, pure following waves cannot

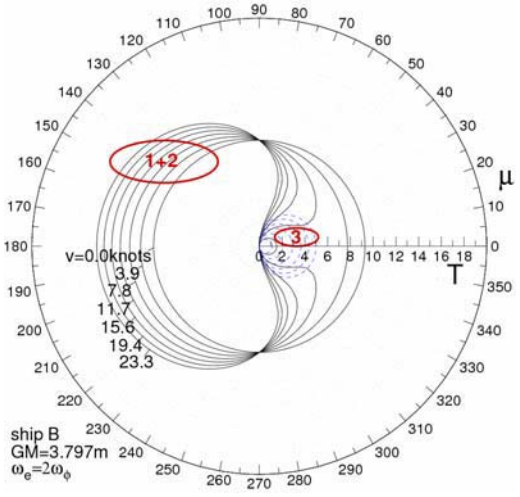

Fig. 8. Resonance conditions for low-cycle parametric rolling for Ship B with *GM*=3.797 m

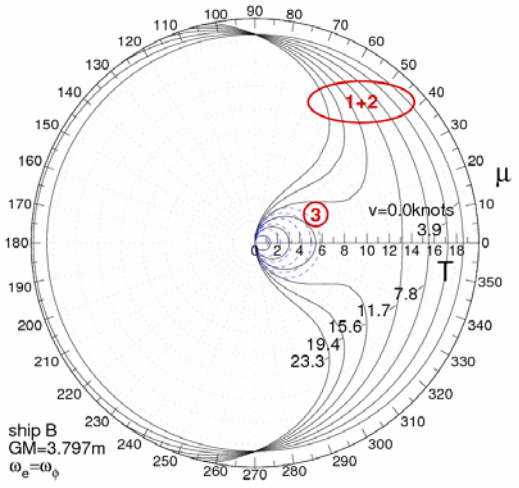

Fig. 9. Conditions for synchronous rolling and fundamental resonance: Ship B, *GM*=3.797 m

In Fig. 8 and 9 lines "1+2" (solid) correspond to conditions 1 and 2, and lines marked "3" correspond to condition 3

lead to the encounter frequency $\omega_e = 2\omega_\varphi$ for the speeds larger than $g/(8\omega_\varphi)$, and the suitable areas for resonance shift towards stern-quartering waves. The larger the ship speed, the more the resonance line is shifted towards beam waves, with the minimum wave encounter angle defined as $\cos^{-1}\left[g/(4v\omega_\varphi)\right]$.

The second condition for parametric resonance is related to the fact that maximum changes of righting levers occur if the mid-ship is located on a wave crest when bow and stern are located in neighbour troughs and vice versa. In longitudinally running waves, this means that the wave length should be close to the ship length. Depending on the hull form and the strength of the coupling of roll with pitch and heave motions, this condition usually leads to a range of the critical wave lengths, from about 0.5 to 2 ship lengths (in longitudinally running waves).

In oblique waves, bow and stern lie in the neighbour wave troughs (or stay on the neighbour wave crests) if the wave length is $\lambda_w = L_{pp}\cos\mu$, or taking a range of wave lengths,

$$\frac{L_{pp}}{2}\cos\mu < \lambda_w < 2L_{pp}\cos\mu. \qquad (34)$$

On the polar plot, this condition is satisfied in two domains, one corresponding to bow and the other to stern waves, as shown in Fig. 10 for the case with *GM*=3.797 m.

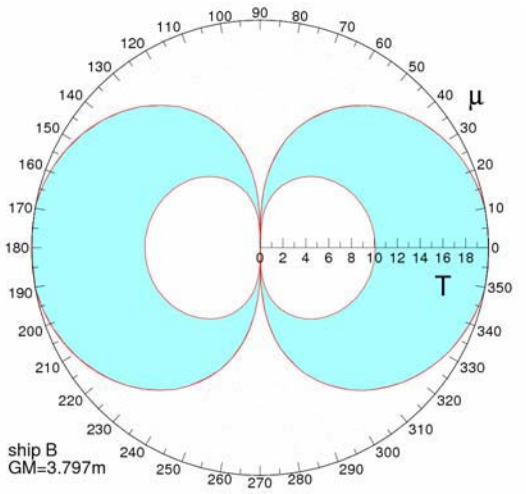

Fig. 10. Suitable wave lengths for parametric rolling according to (34) for Ship B with *GM*=3.797 m

Combining the two conditions of low-cycle resonance on a single plot (see Fig. 11), the areas of possible low-cycle parametric rolling can be identified as the parts of the resonance lines lying within the suitable wave length areas (shown in red in Fig. 11). For this load case, parametric rolling in waves coming from stern directions appears possible only in stern-quartering waves. Following waves satisfying the low-cycle resonance condition are too short for the wave length condition (34) for all ship speeds. Also,

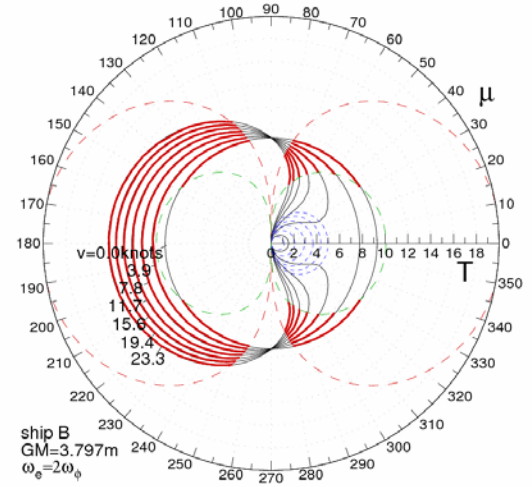

Fig. 11. Combined resonance and wave length conditions for Ship B with *GM*=3.797 m

for low ship speeds (see e.g. 0 knots), low-cycle parametric rolling in waves from bow directions seems also to be possible only in bow-quartering waves because of the same reason.

Conditions for synchronous rolling and fundamental parametric resonance will be considered below.

9.2. Influence of GM

In Fig. 12, the critical areas are shown for the case *GM*=0.88 m. Only the resonance lines corresponding to the low-cycle parametric resonance condition $T_e = T_\varphi / 2$ are plotted, as the condition $T_e = T_\varphi$ leads for this load case to very large wave periods, which are out of the range shown in Fig. 12 and are also not critical in a real seaway. The resonance lines are plotted for seven uniformly distributed ship speeds from 0 to 23.3 knots. Resonance lines corresponding to short waves overtaken by the ship are not shown, as such waves are too short to represent any danger in a real seaway. The lines corresponding to the minimum and maximum critical wave lengths (34) are shown with dashed lines. Parametric rolling is possible in following waves for speeds up to about half of design speed. For larger speeds, resonance shifts towards

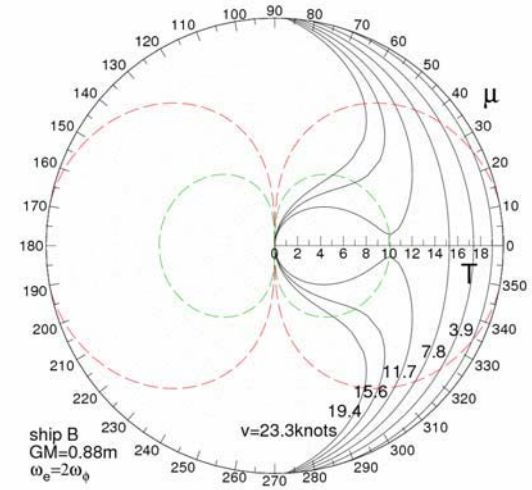

Fig. 12. Critical areas for Ship B, *GM*=0.88 m

stern-quartering waves coming from the directions up to about 50 degrees.

With increasing *GM*, the natural roll period decreases and the lines corresponding to the resonance are 'compressed' towards the origin $T = 0$ of the polar plots. Therefore, synchronous rolling becomes more relevant than for the considered case, while low-cycle parametric resonance will correspond to increasingly shorter waves – above some *GM*, to the waves which do not represent any danger in a real seaway.

For *GM*=1.95 m (see Fig. 13), low-cycle parametric rolling in bow waves becomes relevant, as the resonance lines pass through the area of suitable wave lengths for all ship speeds. On the other hand, low-cycle parametric rolling in stern-quartering waves becomes less critical, as the corresponding wave periods are approximately 6 to 10 s. The synchronous rolling condition $T_e = T_\varphi$ is possible for the considered range of wave periods only for rather small wave encounter angles and large ship speeds, therefore synchronous rolling does not seem to be important for this load case, although fundamental parametric resonance may be relevant.

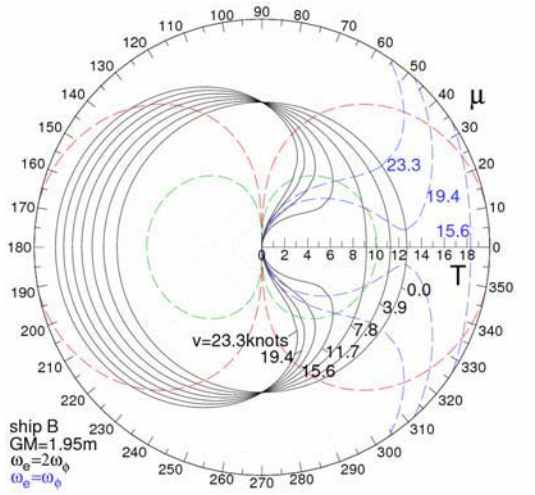

Fig. 13. Critical areas for Ship B, *GM*=1.95 m

For *GM*=3.797 m (see Fig. 8 and Fig. 9), low-cycle parametric roll in head waves becomes less critical as the resonance lines approach the lower boundary of the suitable wave lengths range for small speeds. For larger speeds, parametric rolling in bow waves is usually less critical: if such speeds are achievable, roll damping is sufficiently high. Low-cycle parametric rolling in stern-quartering waves corresponds to rather short waves to represent a significant danger in a real seaway. Synchronous rolling in beam waves corresponds to wave periods of about 18 s, therefore is unlikely to be important. However, fundamental parametric resonance can occur in following (for low speeds) or stern-quartering (for higher speeds) waves.

The case Ship B with *GM*=7.5 m (see Fig. 14) was considered as an example of an extremely high GM. For this load case, low-cycle parametric rolling is unlikely as the corresponding waves are too short. On

the other hand, synchronous rolling condition corresponds to beam waves with periods of about 13 s, thus becoming important.

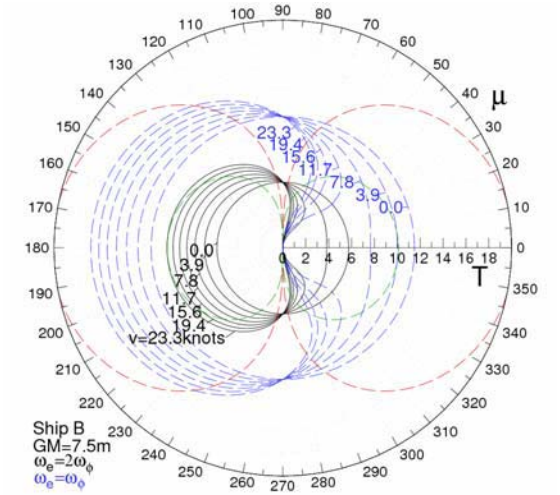

Fig. 14. Critical areas for Ship B, *GM*=7.5 m

9.3. Verification

The results of the above simple considerations were compared with numerical simulations with the nonlinear seakeeping code rolls, for the load cases shown in Table 1. Calculations were carried out in regular waves. The examples of results are shown in Fig. 15 to Fig. 18 as polar plots of roll amplitude from 0 to 30° in axes T (wave period) – μ (wave direction). The plots also show the lines corresponding to resonance conditions for low-cycle parametric resonance ($T_e = T_\varphi / 2$) and synchronous rolling or fundamental parametric resonance ($T_e = T_\varphi$), in black and blue, respectively, as well as

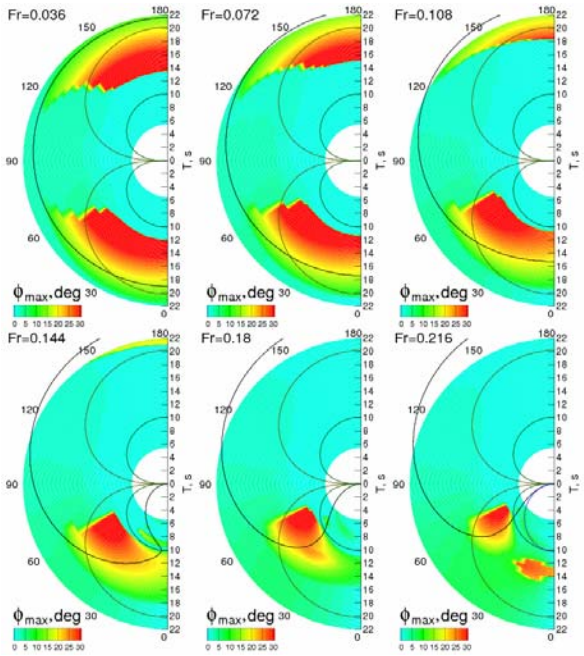

Fig. 15. Roll amplitude in regular waves for Ship B, *GM*=0.88 m

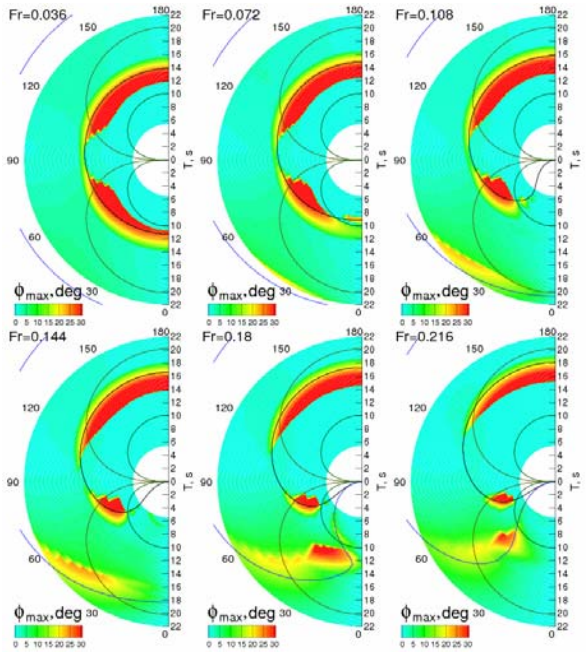

Fig. 16. The same as in Fig. 15, *GM*=1.95 m

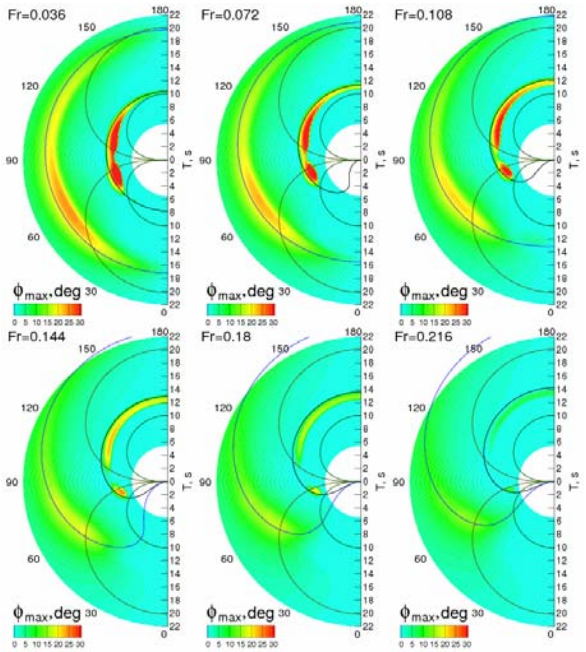

Fig. 17. The same as in Fig. 15, *GM*=3.797 m

the lower and upper boundaries of the area of suitable wave lengths defined by eq. (34) (green and red lines). Each figure shows six polar plots, corresponding to the speeds of 1/6, 1/3, 1/2, 2/3, 5/6 and full design speed (Froude numbers are indicated).

The long-wave boundaries of the low-cycle resonance areas (boundaries with the maximum wave period) follow the resonance line $T_e = T_\varphi / 2$, because these boundaries correspond to the onset of parametric rolling, i.e. rolling with small amplitudes. The small deviations of these boundaries from the resonance lines are due to the difference of the natural frequency of small roll oscillations in the simulations by rolls and the linear roll frequency used for plotting the

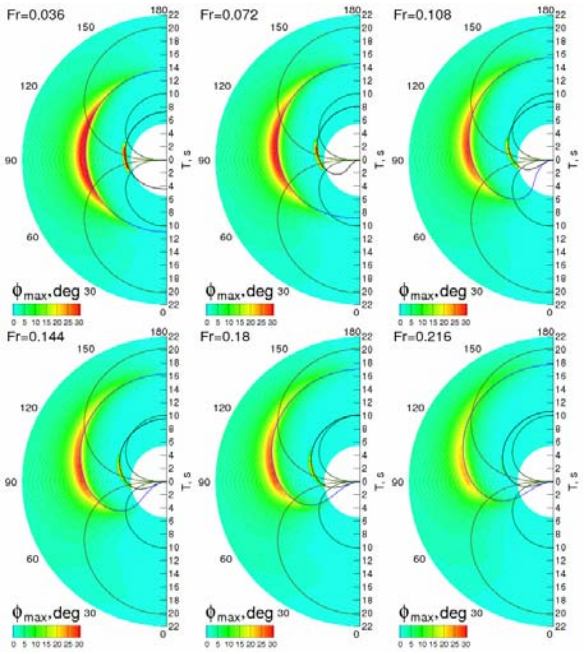

Fig. 18. The same as in Fig. 15, *GM*=7.5 m

resonance lines (found from calculations with a linear frequency-domain strip method GL Strip).

In shorter waves, low-cycle parametric resonance increases (i.e. the red areas on the polar plots are shifted from the resonance condition lines towards the origin $T = 0$), because the natural roll frequency increases with roll amplitude for the considered load cases (as can be seen in Fig. 7).

The condition of the suitable wave length (34) seems to bound the areas of low-cycle parametric resonance rather well, although the area of parametric roll excitation may be broader or narrower than the boundaries described by (34) depending on wave height and forward speed (hence, roll damping).

Synchronous rolling is especially strong in beam waves, see Fig. 18. However, for *GM*=3.797 m (Fig. 17), the peak response shifts towards stern-quartering waves. On several occasions, ship responses were identified which can be attributed to fundamental parametric resonance, e.g. for *GM*=0.88 m (Fig. 15, *Fr*=0.216) and 1.95 m (Fig. 16, *Fr*=0.18 and 0.216).

Results of numerical simulations in irregular waves also confirm the existence and location of the critical areas. Colour maps of the maximum roll angle for 8 hours of simulation time as function of the wave direction μ and mean wave period T_1 are shown below for Ship B with *GM*=0.88 (see Fig. 19), 1.95 (Fig. 20) and 7.5 (Fig. 21) m.

In all these cases, simulations were carried out for long-crested irregular waves with a JONSWAP spectrum and significant wave height h_s=8.0 m.

In bow and, to a larger degree, in following and stern-quartering waves, the area of large roll responses is stretched in radial (wave period) direction compared to the responses in regular waves. This is due to the finite breadth of spectrum in irregular waves: the high-frequency tail of the spectrum has sufficient energy to

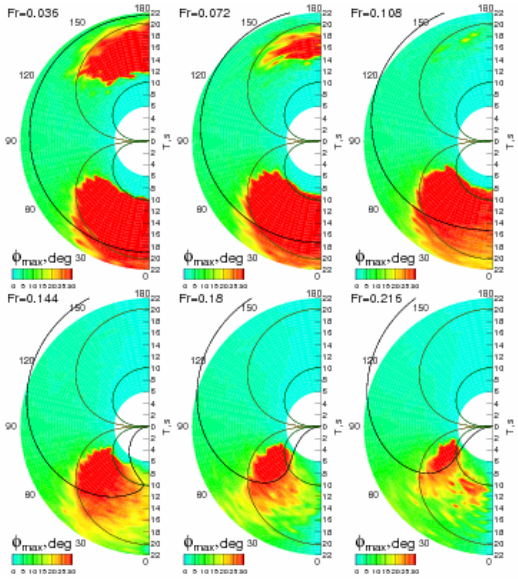

Fig. 19. Critical areas in irregular long-crested waves for Ship B, *GM*=0.88

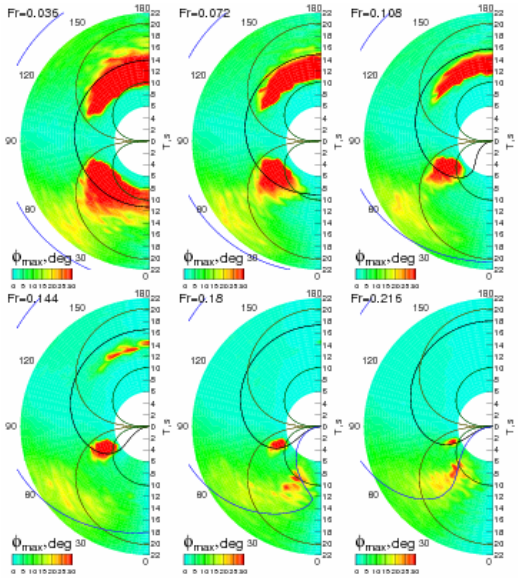

Fig. 20. The same as in Fig. 19 for *GM*=1.95 m

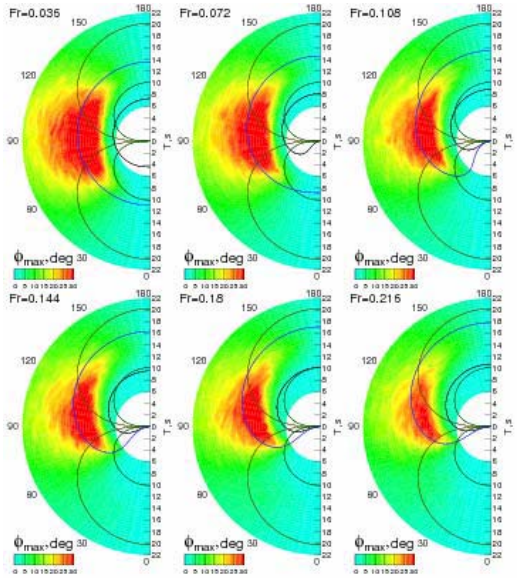

Fig. 21. The same as in Fig. 19 for *GM*=7.5 m

excite parametric or synchronous rolling even if the peak periods of the spectrum are large.

One more factor relevant in irregular stern waves is that the encounter wave spectrum is narrower than the wave spectrum because of the Doppler effect. As a corresponding criterion, one may consider the derivative $\mathrm{d}\omega_e/\mathrm{d}\omega$: if it is small, a larger part of seaway spectrum energy contributes to the excitation around ω_e .

Comparison with experiments for Ship B with *GM*=0.88, 1.95 and 7.5 m confirms the existence of low-cycle parametric resonance in stern-quartering (Fig. 2) and bow (Fig. 3) waves, as well as synchronous rolling in beam waves (Fig. 4), where numerical simulations have predicted them.

9.4. Influence of Forward Speed

An important factor for the assessment of excessive rolling is the decrease of roll amplitude with increasing speed. Fig. 22 shows a comparison of simulation results in regular and long-crested irregular waves: roll amplitude (for regular waves) and standard deviation of roll angles (in irregular waves). The two top plots show dependencies on wave period for fixed Froude numbers; the two bottom plots show the same results re-plotted as dependencies on Froude number for fixed wave periods.

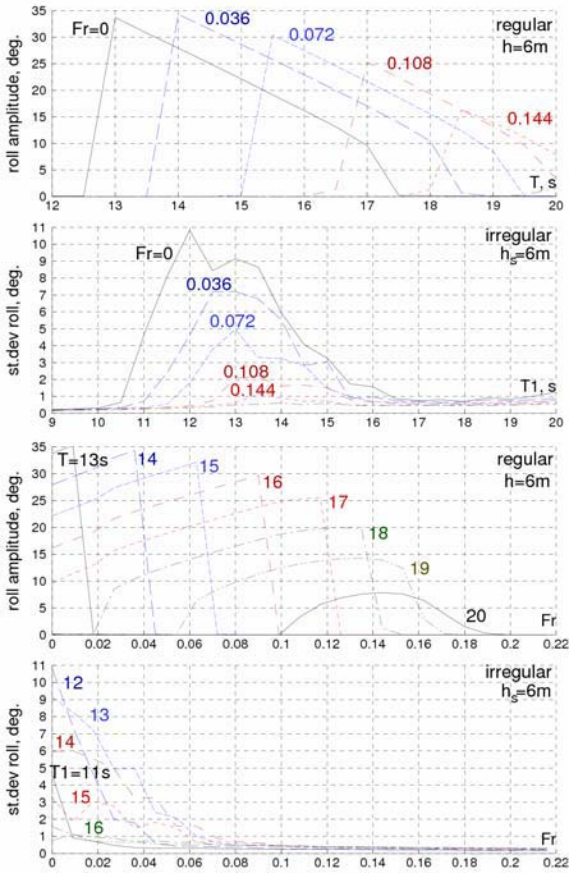

Fig. 22. Roll vs. wave period and Froude number

Dependence of roll amplitude and standard deviation of roll angles on wave period or mean wave period and Froude number for Ship B with *GM*=1.26 m

There are significant differences between regular and irregular waves: the dependencies of roll amplitude on wave period in regular waves are typical for a nonlinear system for which stiffness increases with increasing excitation. With decreasing wave period, roll amplitude first increases slowly, but then drops abruptly to zero. With increasing Froude number, the entire dependency shifts towards longer waves; roll amplitudes decrease slowly because of increasing roll damping. In irregular waves, the dependency of standard deviation of roll angles on mean wave period does not show such an abrupt drop with decreasing T_1 . With increasing Froude number, roll responses decrease much quicker than in regular waves.

Similar difference can be seen in the polar plots in Fig. 23, showing roll amplitude (in regular waves) or maximum roll amplitude (for 8 hours in irregular waves) as a function of wave direction and period or mean wave period. The two top plots show results for two Froude numbers in regular waves, the two bottom ones the corresponding results for irregular waves. Each pair of plots shows results for a smaller (left) and a larger (right) Froude number. These results confirm the tendencies seen in Fig. 22: in regular waves,

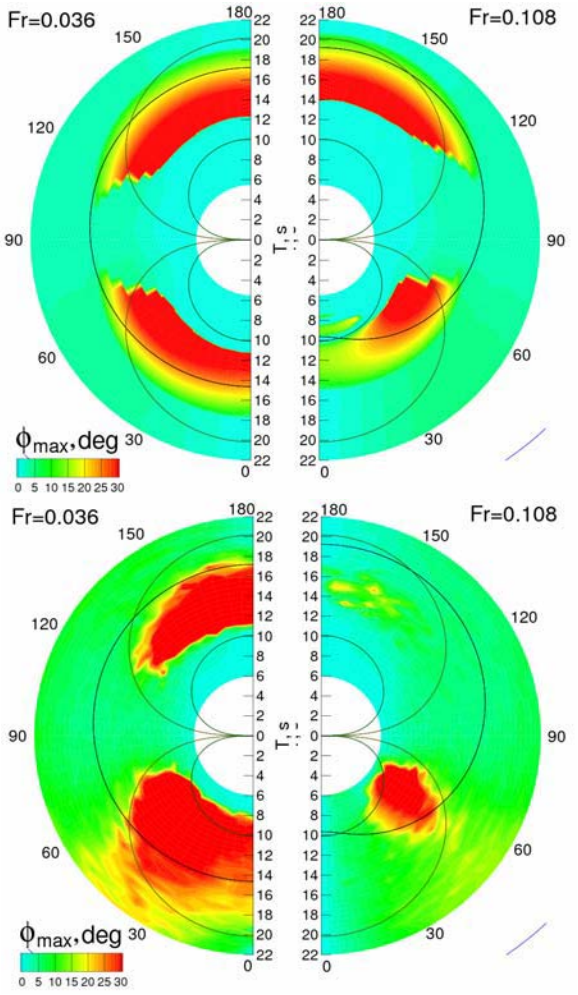

Fig. 23. Maximum roll angle vs. wave period and direction for two Froude numbers

Regular waves (top) and and irregular long-crested waves (bottom); for two Froude numbers: 0.036 (left) and 0.108 (right) for Ship B with *GM*=1.26 m

increasing Froude number shifts the critical area according to changing encounter frequency with a slight decrease of roll amplitudes. In irregular waves, this shift happens together with a large reduction of roll responses. Thus, the effect of increasing Froude number on low-cycle parametric roll responses seems to be much stronger in irregular waves.

Experimental verification of the described differences can be seen in Fig. 24, showing the dependence of roll amplitude in regular waves (top plot) and maximum roll angle in irregular waves (bottom plot) on Froude number for different wave periods (different symbols).

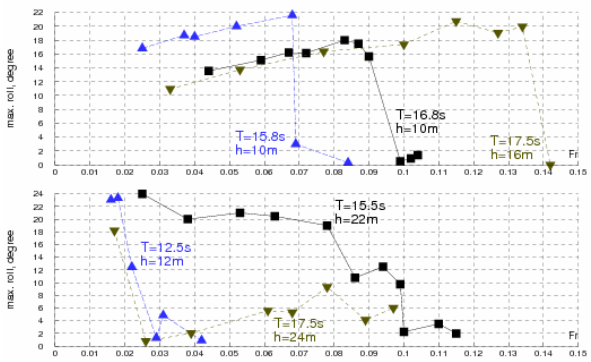

Fig. 24. Measured roll intensity vs. Froude number

Roll amplitude in regular waves (top) and maximum roll angle in irregular long-crested waves (bottom) vs. Froude number for Ship B with *GM*=1.26 m (experiment)

10. Methodology of Numerical Simulations

10.1. Test Cases

The aim of this section is to define how to calculate the short-term exceedance rate r, i.e. the exceedance rate for a given set of seaway conditions h_s, T_1 and operational parameters μ, v. For numerical studies, the test cases listed in Table 4 were used, selected as sections with constant μ over the critical areas found in section 9. For each test case, simulations were carried out for a wide range of mean wave periods, covering the area of excessive roll motions, and a range of significant wave heights from 1 to 20 m.

Table 4. Test cases used for the derivation of the methodology of numerical simulations

test case	ship	*GM*, m	φ_{max}, °	μ, °	Fr
1	B	0.88	26	310	0.108
2	B	1.95	23	170	0.108
3	B	7.5	13	90	0.072
4	B	3.797	19	120	0.108
5	B	3.797	19	80	0.108
6	B	3.797	19	70	0.108
7	C	2.6	18	90	0.09
8	C	2.6	18	90	0.225
9	C	0.67	25	170	0.09
10	C	0.67	25	170	0.27
11	C	0.67	25	60	0.09
12	C	0.67	25	60	0.27
13	A	3.8	22	170	0.108
14	A	2.68	24	55	0.108
15	A	2.68	24	55	0.216
16	A	2.68	24	65	0.216
17	A	2.68	24	35	0.216

10.2. Poisson Processes

To model random events that occur independently of each other, a model of the *Poisson counting process* is often used. The following conditions are required for a counting process to be a Poisson process:

- orderness: only one event can happen at a given time
- the probability of event happening at a particular time instant is infinitely small
- events are independent of each other.

While the first two conditions are satisfied for roll motion, the last condition is questionable, as upcrossings of a certain roll angle tend to appear in groups. The way of performing numerical simulations avoiding the interdependency of upcrossings will be described below.

The following property of stationary (i.e. r is constant in time) Poisson processes is useful:

$$p\{N(\Delta t)=1\} = r\Delta t + o(\Delta t), \text{ while} \qquad (35)$$
$$p\{N(\Delta t)>1\} = o(\Delta t)$$

for a small time interval Δt, where $N(\Delta t)$ is the number of events during this interval.

Conditions (35) can be reformulated as follows: the number of events in any time interval $(t, t+\tau]$ follows a Poisson distribution with the mean $r\tau$, i.e.

$$p\{N(t+\tau)-N(t)=n\} = e^{-r\tau}(r\tau)^n/n!, \qquad (36)$$

for $n=0,1,\ldots$. It follows from (36) that for a homogeneous Poisson process the time intervals between events are exponentially distributed with the parameter r: the time interval τ_1 until the first event is less than some value t if and only if the number of events before t is 0, i.e.

$$p\{t<\tau_1\} \equiv p\{N(t)=0\} = e^{-rt}(rt)^0/0! = e^{-rt}, \qquad (37)$$

i.e. the waiting time until the first event is exponentially distributed. As time intervals between events are independent, all time intervals are random exponentially distributed variables. For an exponential distribution, the probability density function (p.d.f.) $f_t = \mathrm{d}p/\mathrm{d}t$, where $\mathrm{d}p$ is the probability of the event happening in the time interval $(t, t+\mathrm{d}t]$, can be found as $f_t = re^{-rt}$ for $t \ge 0$ and 0 otherwise, and the expected time interval between two events is

$$E_t = \int_0^{+\infty} t f_t(t)\,\mathrm{d}t = \int_0^{+\infty} tre^{-rt}\,\mathrm{d}t = 1/r. \qquad (38)$$

10.3. Methodology of Simulations

Because of the strong auto-correlation of large-amplitude roll motions, time averaging is unsuitable for the definition of the exceedance rate. Therefore following *Söding (1987)*, each calculation was continued only until the first exceedance event at time instant t_1. Then the ship was returned to the upright position, and the simulation was repeated again until the next exceedance event etc. The estimation of the expected upcrossing period is found from the results of n numerical simulations as $\tau = \frac{1}{n}\sum_{i=1}^{n} t_i$, and the estimation of the expected exceedance rate is calculated as $r = 1/\tau$.

Using this method, care should be taken of too small exceedance periods: if an exceedance event occurs too quickly after the start of the simulation, the influence of the initial conditions may be too large. Therefore, all exceedance periods smaller than a given threshold $t_0 = n_\varphi T_\varphi$ are neglected in the averaging. Here, n_φ is prescribed, and T_φ is the average roll period in the simulation. This in turn can lead to wrong results if the expected upcrossing period is small: if we assume the upcrossing periods as exponentially distributed, omitting exceedance periods below t_0 shifts the estimation $\hat{\tau}$ to the right from the expected exceedance period E_t. To compensate for this inaccuracy, this estimation found from simulations is corrected as $\tau = \hat{\tau} - t_0$, where $\hat{\tau}$ is the average exceedance period defined from numerical simulations neglecting exceedance periods less than t_0.

Estimation of the average exceedance period or exceedance rate directly requires large simulation time as the standard r_f is small. A method to accelerate simulations when exceedance rate is too low is to extrapolate the exceedance rate over significant wave height according to *Tonguć and Söding* (1986). The method is based on the assumption that rare excessive roll amplitudes occur because of few large waves, which satisfy Rayleigh distribution. Assuming that excessive roll amplitudes occur with a certain unknown probability if a certain unknown number of successive wave amplitudes exceed a certain (also unknown) limit, leads to the following relation for the exceedance rate per roll period $r_\varphi = rT_\varphi$:

$$-\ln r_\varphi = A + B/h_s^2 \,. \tag{39}$$

This method works also for parametric and synchronous rolling, although the number of successive large waves required to excite large roll angles may differ for the different phenomena (which means that the parameters A and B in (39) vary with wave direction and period, as well as ship speed).

An example of the calculated estimations of the average exceedance rate for test case 2 is shown in Fig. 25. The dependencies of $-\ln r_\varphi = -\ln\left(T_\varphi/\tau\right)$ on $1/h_s^2$ are shown for different mean seaway periods T_1. Results of numerical tests for the cases listed in Table 4 show that the minimum required number of simulations for the estimation of the average exceedance rate n is approximately 150.

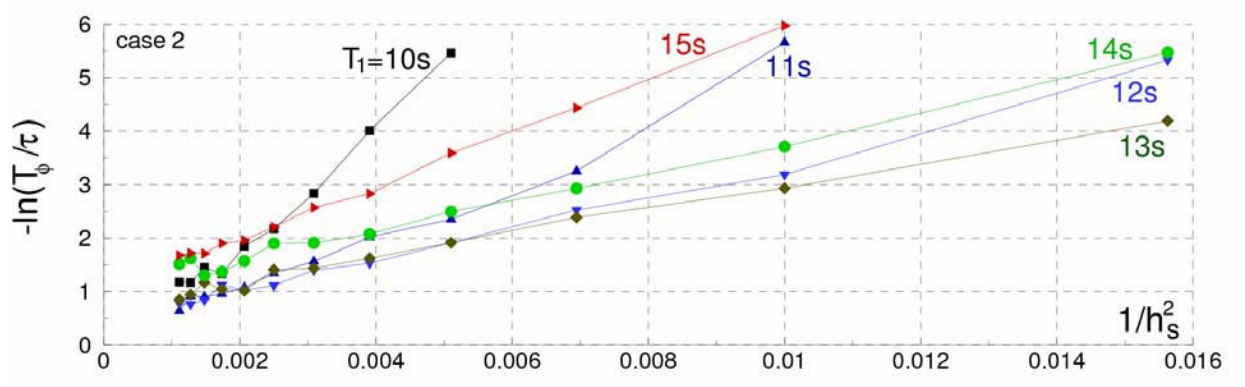

Fig. 25. Average exceedance rate vs. significant wave height for test case 2

The example in Fig. 25 and results for other test cases show that the dependencies of $-\ln r_\varphi$ on $1/h_s^2$ become linear for all considered load cases, seaway conditions and operational parameters if h_s is sufficiently small, including cases of parametric and synchronous rolling. The results indicate that linear dependency can be used for the extrapolation over significant wave height for $-\ln r_\varphi > 4$, or $\tau = T_\varphi/r_\varphi > 50T_\varphi$; if 150 simulations are used, the total simulation time would be $7500 \cdot T_\varphi$, which is acceptable for simulations with rolls.

11. Design Assessment Procedures

The introduced design assessment procedure is based on finding $r_f^{\max}$ for all possible wave directions, periods and heights. The conditions (wave direction, mean wave period and significant wave height) maximising $r_f^{\max}$ are referred to as critical. The wave directions for test cases 1 to 17 listed in Table 4 were selected as cuts through critical areas, while the critical wave heights and periods were found directly

from simulations. The probability density function of seaway parameters f_{h_s,T_1} was calculated from the annual average seaway probabilities for the North Atlantic according to *Söding (2001)*. A summary of the results is shown in Table 5 including case number, critical seaway period and wave height (a range is shown), and the calculated $r_f^{\max}$. The ratio of the critical mean wave encounter period to the natural roll period was found to vary from 0.3 to 0.5 for low-cycle parametric resonance and from 0.7 to 1.0 for synchronous rolling and fundamental parametric resonance.

Table 5. Summary of design assessment studies

case	T_1^*, s	h_s^*, m		$r_f^{\max}$	h_s^d, m	τ, s	T_φ, s
1	11.0	7	8	1.723E-04	10.731	81.493	30.77
2	13.0	10	12	1.094E-05	13.794	179.133	23.73
3	11.0	7	8	2.492E-04	10.731	43.21	11.97
4	15.0	12	14	4.580E-07	16.775	562.112	17.56
5	15.0	12	14	9.683E-07	16.775	354.013	17.73
6	15.0	12	14	9.727E-07	16.775	328.69	17.77
7	9.0	5	6	5.750E-04	7.755	31.462	8.96
8	8.5	5	6	7.560E-06	7.045	202.622	9.36
9	9.0	5	6	2.303E-04	7.755	73.582	15.71
10	9.0	7	8	5.974E-08	7.755	61343.284	-
11	13.0	10	12	3.604E-06	13.794	235.128	16.37
12	12.0	10	12	1.242E-07	12.262	2348.948	16.76
13	12.5	10	12	4.155E-08	13.029	10699.06	20.9
14	11.0	9	10	6.144E-09	10.731	64461.538	-
15	17.0	16	18	7.369E-08	19.505	981.318	27.11
16	17.0	16	18	1.057E-08	19.505	5668.57	19.74
17	16.0	14	16	8.543E-08	18.182	1327.157	27.81

This design assessment procedure does not need much computing time, but requires the identification of critical areas and calculation of the parameters A and B. In addition, the resulting $r_f^{\max}$ depends on the selected seaway scatter table.

A simplified method was tested, namely carrying out simulations for a single significant wave height per wave period $h_s^d(T_1;\mu,v)$. The dependency of h_s^d on T_1 is defined from the seaway frequency table as an approximation of a line with a constant (very small) seaway probability density. Because for all simulations along this line $f = \text{const.}$, the exceedance rate itself (or exceedance period) can be used directly as a design assessment criterion. Here, the approximation proposed by Söding in *SLF 50/Inf.2 (2007)* was used:

$$h_s = (0.013 - 0.00036 \cdot T_1) \cdot g T_1^2 , \qquad (40)$$

shown in Fig. 26 together with critical wave height according to Table 5.

Results of the simulations are shown also in Table 5, including 'design wave height' according to the approximation (40), estimation of the expected exceedance period τ from numerical simulations, and the average roll period T_φ.

Ranking of the test cases by these two assessment procedures is shown in Table 6. The first two

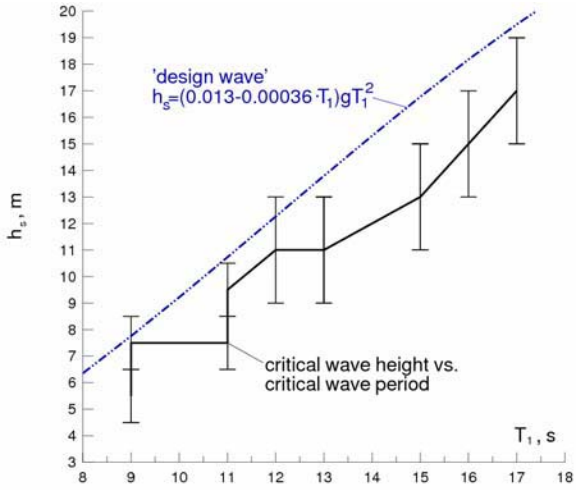

Fig. 26. Critical wave height vs. critical seaway period according to Table 5 and formula (40)

columns show the case number and the maximum r_f obtained by the full search over T_1 and h_s; the test cases are sorted from the lowest r_f to the highest. The third and fourth columns show the test case number and the estimated mean exceedance period obtained from the simulations with the 'design wave height' (40). The ranking by the two methods agrees well; some disagreements occur for the safest test cases. It appears that the standards can be selected in the range of test cases 4, 5 and 6, $R_1 = 10^{-6}$, and the standard average exceedance period for the simplified assessment method 500 s.

Table 6. Summary of design assessment studies

maximum r_f		design wave (40)	
case	r_f, s^{-1}	case	$\hat{\tau}$, s
14	$6.144 \cdot 10^{-9}$	14	64461.538
16	$1.057 \cdot 10^{-8}$	10	61343.284
13	$4.155 \cdot 10^{-8}$	13	10699.06
10	$5.974 \cdot 10^{-8}$	16	5668.57
15	$7.369 \cdot 10^{-8}$	12	2348.948
17	$8.543 \cdot 10^{-8}$	17	1327.157
12	$1.242 \cdot 10^{-7}$	15	981.318
4	$4.58 \cdot 10^{-7}$	4	562.112
5	$9.683 \cdot 10^{-7}$	5	354.013
6	$9.727 \cdot 10^{-7}$	6	328.69
11	$3.604 \cdot 10^{-6}$	11	235.128
8	$7.56 \cdot 10^{-6}$	8	202.622
2	$1.094 \cdot 10^{-5}$	2	179.133
1	$1.723 \cdot 10^{-4}$	1	81.493
9	$2.303 \cdot 10^{-4}$	9	73.582
3	$2.492 \cdot 10^{-4}$	3	43.21
7	$5.75 \cdot 10^{-4}$	7	31.462

12. Application of the Simplified Procedure

Using the simplified design assessment procedure requires little simulation time even for the entire range of wave encounter angles and seaway periods and can be applied without the identification of the critical areas. To demonstrate its application, a series of

simulations has been carried out for all of the load cases listed in Table 1, with the following parameters:

- mean seaway period T_1 between $\max\left(T_\varphi/4, 8\text{ s}\right)$ and $\min\left(T_\varphi, 18\text{ s}\right)$, step 1 s
- significant wave height according to the 'design wave height' (40)
- wave directions from 0 to 180° every 10°
- speeds 0.5, 0.75 and 1.0 of design speed

The simulation time was set to 105 s for all cases. Results of these calculations are shown in Table 7 (the minimum average exceedance period for the three speeds) and Table 8 (the mean wave direction and mean seaway period corresponding to the minimum exceedance period).

Table 7. Summary of the simplified design assessment

ship	*GM*, m	minimum average exceedance period, s		
		$0.5\cdot v$	$0.75\cdot v$	$1.0\cdot v$
A	2.68	799	658	729
A	3.8	728	1570	3555
A	4.57	815	2422	7675
A	5.88	282	686	2024
B	0.88	62	88	106
B	1.26	267	1523	2759
B	1.95	182	297	372
B	3.797	296	1004	5537
B	7.5	26	27	25
C	0.67	151	429	49982
C	0.82	159	612	33313
C	1.71	47	75	217
C	2.54	28	44	86

Table 8. Critical seaway conditions for the simplified assessment

ship	*GM*, m	$0.5\cdot v$		$0.75\cdot v$		$1.0\cdot v$	
		μ	T_1	μ	T_1	μ	T_1
A	2.68	170	14	170	18	0	17
A	3.8	60	18	60	17	60	16
A	4.57	60	18	60	17	70	16
A	5.88	100	17	100	18	90	17
B	0.88	0	15	10	16	30	18
B	1.26	180	14	180	15	0	18
B	1.95	180	13	180	14	180	14
B	3.797	80	15	80	16	90	18
B	7.5	110	15	100	13	110	15
C	0.67	180	9	180	9	90	12
C	0.82	170	8	170	9	100	15
C	1.71	110	13	110	13	100	13
C	2.54	90	12	90	13	100	14

The results show high sensitivity of the probabilistic stability measures to the ship speed. Therefore, accurate estimation of the maximum ship speed as a function of wave height, direction and period, as well as of the loading state (including voluntary speed reduction) is necessary. If such data are not available, 0.5 of design speed can be recommended for design assessment as a conservative condition.

13. Operational Guidance

To develop operational guidance, simulations were carried out for Ship B, *GM*=1.26 m in short-crested irregular waves with JONSWAP spectrum ($\gamma = 3.3$).

For each combination of ship speed, wave direction and mean period, simulations were performed for significant wave heights from 20 m in descending order with step 1 m for 10^6 s of simulation time. Parameters A and B were defined from the results of two simulations with the minimum wave heights (denoted h_1 and h_2), for which the number of exceedance events was larger than 150, as

$$A = \frac{h_1^2 \ln\left(\tau_1 / T_{\varphi 1}\right) - h_2^2 \ln\left(\tau_2 / T_{\varphi 2}\right)}{h_1^2 - h_2^2}, \tag{41}$$

$$B = h_1^2 h_2^2 \frac{\ln\left(\tau_2 / T_{\varphi 2}\right) - \ln\left(\tau_1 / T_{\varphi 1}\right)}{h_1^2 - h_2^2}. \tag{42}$$

Using these A and B, the exceedance rate was calculated as a function of significant wave height as

$$r = \exp\left(-A - B/h_s^2\right)/T_\varphi, \tag{43}$$

and the product $r_f = r \cdot f$ was calculated using the seaway probabilities according to *IACS Rec. No.34 (2001)*. The results are graphically represented as maps of the significant wave height for which $r_f = R_2$ as a function of ship speed (radial coordinate) and relative wave heading (circumferential) for different mean seaway periods in Fig. 27.

14. Roll Mitigation

Bilge keels, anti-roll fins and anti-roll tanks can significantly reduce the danger of excessive roll motions and therefore their use should be encouraged by regulations. The following consideration seems conservative enough:

- bilge keels are accounted for in design assessment and in operational guidance. The method by *Gadd (1964)* can be used
- anti-roll fins and tanks are not considered in the design assessment, but are taken into account in the operational guidance, which should be provided for operation with and without these devices.

15. References

Blume, P. (1976) *Zur Frage der erregenden Längskraft in von achtern kommenden regelmäßigen Wellen.* Rep. No.334, Institut für Schiffbau, Hamburg

Blume, P. (1979) Experimentelle Bestimmung von Koeffizienten der wirksamen Rolldämpfung und ihre Anwendung zur Abschätzung extremer Rollwinkel, *Schiffstechnik* **25**(1), 3-29

Balcer, L. (2004) Location of ship rolling axis, *Polish Maritime Research* **11**(1), 3-7

Gadd, G. E. (1964) *Bilge keels and bilge vanes*, Report Nr. 64, Ship Div., National Physical Lab.

GL's Rules for Classification and Construction (2006) Volume I. Ship Technology

Grim, O. (1961) Beitrag zu dem Problem der Sicherheit des Schiffes im Seegang, *Schiff und Hafen* 490

IACS Rec. No.34 (2001) *Standard Wave Data*

Kröger, P. (1987) Roll Simulation von Schiffen im Seegang, *Schiffstechnik* **33**(4), 187-216

Petey, F. (1986) Forces and moments due to fluid motions in tanks and damaged compartments, *Proceedings, 3rd Int. Conf. on Stability of Ships and Ocean Vehicles STAB'86*, Gdansk

SLF 50/INF.2 (2007) Proposal on additional intact stability regulations. – Submitted by Germany26 January 2007

Söding, H. (1982) *Leckstabilität im Seegang.* Rep. No.429, Institut für Schiffbau

Söding, H. (1987) Ermittlung der Kentergefahr aus Bewegungssimulationen, *Schiffstechnik* **34,** 28-39.

Söding, H. (2001) Global seaway statistics, *Ship Techn. Res.* **48,** 147-153

Tonguć, E. and Söding, H. (1986) Computing capsizing frequencies of ships in a seaway, *Proceedings, 3rd Int. Conf. on Stability of Ships and Ocean Vehicles STAB'86*, Gdansk

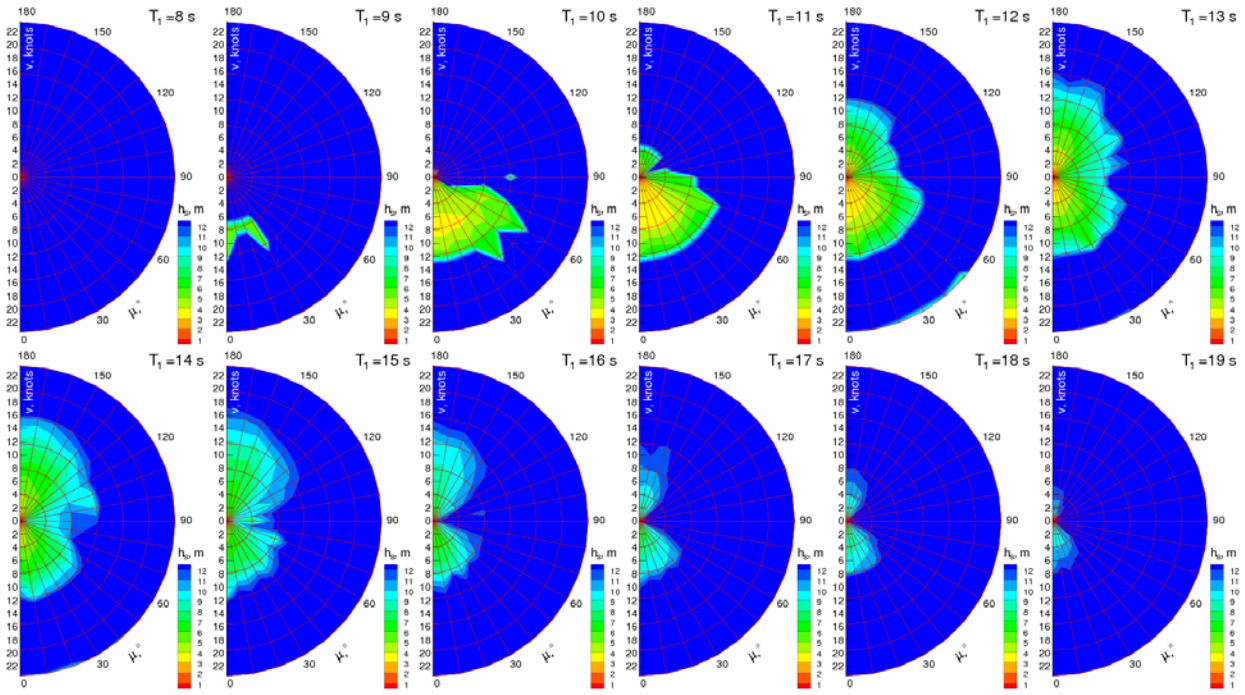

Fig. 27. Operational guidance: Ship B, *GM*=1.26 m

Maximum allowed significant wave height vs. ship speed in knots (radial coordinate) and wave direction (circumferential coordinate) for different mean seaway periods